2012

Thermal Analysis of a Solar Cavity Receiver

Yuvraj Singh
Lehigh University

Thermal Analysis of a Solar Cavity Receiver

By

Yuvraj Singh

A Thesis

Presented to the Graduate and Research Committee

of Lehigh University

In Candidacy for the Degree of

Master of Science

In

Mechanical Engineering

Lehigh University

July 2012

This thesis is accepted and approved in partial fulfillment of the requirements for the Master of Science in Mechanical Engineering

Thermal Analysis of a Solar Cavity Receiver by

Yuvraj Singh.

_____

Date Approved

_____

Dr. Sudhakar Neti
Principal Advisor

_____

Dr. Gary Harlow
Department Chair

Acknowledgements

I would like to take the time to thank the Department of Mechanical Engineering, the faculty and staff for my intellectually stimulating and engineering enriched education at Lehigh University.

Thank you to Dr. Alparslan Oztekin with help in the formulation and solution of this problem. Thank you to my lab mates in the Oztekin Computational Fluid Mechanics group, for the usage of their high performance computing equipment to undertake my intensive simulations.

Thank you to Dr. Sudhakar Neti for the chance to complete my masters thesis in the exciting field of solar energy.

Lastly thank you to my parents who have funded my education and stay at Lehigh University as an undergraduate and graduate student, allowing me to complete this thesis in the comfort of their home.

TABLE OF CONTENTS

LIST OF FIGURES

TERMINOLOGY and NOTATION

L	Length of Cavity Receiver	ρ	Density of Fluid
Dc	Diameter of Cavity Receiver	v	Inlet Velocity of Fluid
Da	Diameter of Aperture	μ	Viscosity of Fluid
d_i	Diameter of Coil Pipe	Re_D	Reynolds Number
Do	Diameter of Helical Coil	cp	Specific Heat of Fluid
Lc	Length of Helical Coil	k	Thermal Conducitivty of Fluid
Dr	Diameter of Reflector	Pr	Prandtl number
θ	Angle of Interest	$Re_{critical}$	Reynolds Critical
A_i	Area of Surface	Nu_D	Nusselt number
ε_i	Emissivity of Surface	l	Length of Cavity Receiver to Length of Helical Coil (L/Lc)
qsolar	Incoming Solar Input	h	Length of Cavity Receiver to Diameter of Cavity Receiver (L/Dc)
h_2	Heat Convection Coefficent of Aperture	e	Length of Cavity Receiver to Diameter of Aperture (L/Da)
hf_i	Heat Convection Coefficent of Working Fluid	a	Diameter of Cavity Receiver to Diameter of Aperture (Dc/Da)
Tf_i	Fluid Temperature	b	Diameter of Cavity Receiver to Diameter of Helical Coil (Dc/Do)

T_∞	Free Stream Temperature	c	Diameter of Helical Coil to Diameter of Aperture (Do/Da)
kf	Thermal Conductivity of Insulation of Lid, Reflector	δ	Diameter of Helical Coil to Diameter of Coil Pipe (di/Do)
t	Thickness of Insulation of Lid, Reflector	N	Number of Turns in Helical Coil (Lc/di)
q_i	Net Heat Transfer Rate from Surface	E_{gen}	Energy Generated
J_i	Outgoing Heat Transfer from Surface	σ	Stefan Boltzmann's Constant
G_i	Incoming Heat Transfer to Surface	$\in$	Efficiency
Eb_i	Blackbody Emissive Power of Surface	R	Distance Between Surfaces for View Factor Calculation
Tfo_i	Outlet Temperature of Fluid	F_{ij}	View Factor Relationship Between Surfaces
Tfi_i	Inlet Temperature of Fluid	T_{mi}	Mean Temperature of Fluid
$\dot{m}$	Massflow Rate of Fluid		

<u>Abstract</u>

Design of solar thermal cavity receivers has been a subject of interest for the renewable energy community. The ability to harvest solar energy through fluid-thermal interactions, not only provides a viable, efficient, and environmentally friendly source of power, but also one which reduces the cost of implementing and generating the power needs of today.

The following investigation develops a simulation of the thermal and heat transfer behavior of a solar cavity receiver. The model constructed treats the convective and radiative exchange as the main component to energy capture of solar energy within the system.

The results show that tightly packed cavity receivers exhibit higher working fluid temperatures for both laminar and turbulent conditions in comparison to medium and loosely packed cavity receivers. Tightly packed cavity receivers demonstrate net heat transfer distributions with local maxima, with highest net heat transfer in the middle of the cavity receiver, in comparison to loosely packed systems, which have decreasing linear-like net heat transfer distributions with increasing fractional cavity receiver depth for both laminar and turbulent flow conditions.

It is demonstrated that further increasing the aperture size of the cavity receiver beyond 60 cm, results in lower working fluid temperatures and net heat transfer distributions for varying aperture size for both laminar and turbulent conditions. It was demonstrated that decreasing helical pipe size of the cavity receiver results in higher working fluid temperatures and net heat transfer rates for both laminar and turbulent conditions.

It was based on these observations and conclusions that an optimal cavity receiver design was investigated for three popular heat transfer fluids. A tightly packed cavity receiver with minimized aperture and helical pipe diameters was chosen as the optimal cavity receiver for the three popular heat transfer fluids.

Chapter 1. Introduction

The growing energy needs of today's world, call for not only viable, efficient sources, but also cost effective, environmentally friendly-energy options. Renewable energy sources, as solar, wind, and biomass, offer the options of harvesting nature's glory, despite growing market conditions and developing infrastructure [1].

Solar energy, offers the option to harness solar radiation, whether through automatic conversion to electricity via solar photovoltaic panels or heating of a working fluid in a heat exchanger to generate electricity in a later engineering process stage [1]. The latter of the options is associated with the growing field of solar thermal energy.

Solar thermal energy options offer the ability to capture, collect, and store solar radiation through thermal-fluid based interactions of a working fluid, typically a molten salt or heat exchanger based fluid, within its module and enclosing system [2-3]. Despite initial, high capital investment, solar thermal energy provides efficient solar energy to electricity power generation at maintainable operating costs and controlled conditions [2-3]. It is of the fluid-thermal and design engineers' best interest to choose the appropriate module and system, by which these physical interactions can be controlled and optimized.

One of the many solar thermal technologies, the cavity receivers forms the energy collection modules for point concentrator solar collectors. The goal of this investigation is to study the thermo-fluid behavior of a solar cavity receiver. This investigation aims to understand the radiative exchange from the system, as a result of the ongoing thermal dynamics of the cavity receiver system and also as of the effect of geometric changes in the cavity receiver. This dual analysis allows the results of the investigation to further suggest optimal design conditions for the solar cavity receiver.

In the next few pages, a "Survey of Literature" is presented. This will encompass current research and findings in the solar thermal community. It is the interest of this investigation to produce unique work that will be of importance to the solar thermal energy community and its imperative the reader understand the current, exciting work undergoing in this field.

Continuing on, the next section explains the objective of this investigation. More so, why this investigation is unique and how potentially it may aid the understanding of the solar thermal energy community. Given the initial interest of the reader, then the methodology of analysis is explained. The methodology of analysis is written, assuming the reader has basic understanding of fluid mechanics, heat transfer, and applied mathematics. Experienced heat transfer and fluid mechanics experts may want to briefly read through this section, before spending their time in the "Results and Discussion". Within the methodology of analysis, the solar cavity receiver geometry of interest is outlined and described. A simple theoretical model based on the conservation of energy and radiative exchange between surfaces of interest is explained in detail. Given the wealth of literature on helical coils and the use of these pipes in the solar cavity receiver, appropriate mathematical representations of heat transfer fluid properties as a result of flow in helical coiled pipes is described, with relevant, well known authors cited for their exciting work. Finally in the methodology of analysis, the properties of the heat transfer fluid of analysis are described as well as the appropriate dimensionless variables which guide the analysis of the thermal behavior of the solar cavity receiver.

The subsequent section holds the results and the discussion of the results. The results for 81 different simulation cases as described in Appendix B, in relation to changes in the geometry of the cavity receiver and mass flow rate, Reynolds number, and heat convention coefficient of flow, are displayed in accordance to the change in geometry of the cavity receiver and the effect on the thermal dynamics of the cavity receiver. Appropriate discussion is placed at key junctures as the results are described and analyzed. The analysis of the results is utilized to suggest in the optimal design conditions for a solar cavity receiver given two more additional popular heat transfer fluids.

The conclusion section further details the relative significance of this work as in relation to the findings and their respective analysis and its application to current work in the solar thermal community. Further the conclusion suggests future work and its relation to the current investigation.

In the last sections of this investigation, appropriate appendices are presented, so the reader of interest can further understand and critique the method of analysis of choice. Appendix A contains appropriate view factor relationships for surface-to-surface radiation calculations and Appendix B contains the simulation test cases, as described in the "Results and Discussion". Lastly for the reader's interest, sets of concluding remarks are included.

Chapter 2. Survey of Literature

Only recently has the interest in the development of novel and efficient design of solar thermal cavity receivers to meet the energy needs of the world, been renewed [4-9]. The Solar Hybrid Fuel Project of Japan aimed to develop molten salt solar receivers with novel beam down concentrators. These beam down type solar systems concentrated solar radiation harvested from a heliostat field of 400 m radius responsive to the changes in sun direction and location [4]. The sunlight was concentrated downward into the solar cavity receiver aperture via compound parabolic concentrator, which faced upward [4]. These results were obtained using a numerical simulation code, which determined the temperature distributions of the receiver and the molten salt, from effects of conductive, convective, and radiative transfer in the receiver system. The investigators found that net heat transfer rates in the cavity receiver system exhibited a Gaussian like distribution behavior with net heat transfer the highest in the middle of the cavity receiver [4]. Furthermore the working fluid temperatures reached around 580°C and the solar cavity receiver designs were rated at an efficiency of 90% with thermal output of 100 MW$_{th}$ [4].

The broad exploration of the Solar Hybrid Fuel Project of Japan opened a new chapter in the theoretical and numerical investigations of solar thermal cavity receivers and their design. As interested as groups as the Solar Hybrid Fuel project were in general energy capture and collection in the solar cavity receiver, others were interested in the details that surrounded the losses from the cavity receiver.

Prakash et. al [5] demonstrated that within a cylindrical cavity receiver system of length of 0.5 m and internal diameter of 0.3 m, the convective and radiative heat losses from the working fluid of water between temperatures of 50-150° C, formed the major constituents of the thermal losses [5]. One of the group's chief interests was to numerically understand the heat losses from different orientations of the cavity receiver at 0°, 45°, and 90°, unlike the Hybrid Fuel Project, which orientated the cavity receiver system just at 90° angle. It was found that the convective losses decreased with increases in receiver inclination, while losses increased with increasing mean receiver temperature [5]. Furthermore the investigation of the wind induced convective losses, led the authors

to conclude that head-on-wind of velocity of 1 m/s cause 22-75 % heat losses and head on-wind of velocity of 3 m/s cause 30-140% heat losses from the cavity receiver [5].

Further investigation into the orientation of the cavity receiver was conducted by Kumar and Reddy [6-7], who quantified laminar convective heat losses and radiative heat transfer through a 2D heat loss model for a modified hemispherical cavity receiver. Similar results as Prakash et. al [5] were demonstrated as 52% and 71% of total heat loss was at 0° inclination and 40% and 59% of the total heat loss was at 90° inclination for the modified cavity receiver with an area ratio of 8 at 400°C [6-7].

Fang et. al. [8] approached a similar problem as Kumar and Reddy's investigation through a novel approach of solving for, instead of assuming the wall heat fluxes, within a prism like cavity receiver at an inclination angle of 21.8° with a working fluid of water. The authors utilized the Monte-Carlo method, an intensive iterative method which relies of tracking light rays and determining through a probabilistic means whether or not these light rays are absorbed, reflected, emitted, and/or scattered from the medium or interface of interest [8]. For simplicity of simulation, the scattering by the air medium was neglected [8]. Energy balances were employed, assuming constant temperatures and emissivities, utilizing radiative heat transfer factors as calculated by the Monte Carlo method in the packaged software FLUENT, to solve for the temperatures of the surfaces [8]. It was demonstrated that 48% of the energy gained through solar input was a received by the cavity receiver tubes and 26% gained by the receiver walls [8]. The authors demonstrated the internal wall of the receiver to reach temperatures of 280-640° C and cavity receiver tubes to reach temperatures of 270-430° C [8]. It was further demonstrated that total heat loss increased in wind speed direction of 30-90° and decreased in wind speed direction of 90-120° [8].

With the emergence of researchers with a sincere interest in the understanding of the convective loss nature of cavity receivers, came the alternative interest in the understanding of the radiation dynamics of the solar cavity receiver system. Shuai et. al [9], utilized the Monte-Carlo ray-tracing method, as previously described in Fang et. al [8], to further understand the radiation dynamics of cavity receiver systems. The authors studied cavity receivers of cylindrical, dome, elliptical, spherical, and conical shapes [9].

5

Interestingly it was demonstrated that the spherical cavity receiver exhibited Gaussian like heat flux distribution at its cavity wall with the highest heat flux in the middle of the receiver wall, while the elliptical cavity receiver exhibited Gaussian like heat flux distribution at its cavity wall with the highest heat flux at the end of the receiver wall [9]. The conical receiver was shown to have a Gaussian like heat flux distribution as well, with the highest heat flux at the end of the cavity receiver wall [9].

Interestingly, despite increased interest in the convective and radiative nature of the cavity receiver and detailed analytical and numerical solutions to understand these physical dynamics within the cavity receiver, researchers have neglected the major effects of the inner module, which stores the energy in the working fluid, on thermal analysis, function, and efficiency. Solar cavity receivers contain tubes which are arranged in a number of shapes and formats [4-9]. Helical coils have recently begun to take interest in the design of solar collector modules [5]. It has been well evidenced that flows in helical pipes behave under certain experimental and mathematically defined fluid-thermal characteristics [10-24]. It will be briefly noted that these scientific works on the laminar and turbulent flows in helical pipes are based extensive, diligent experimentation with precise measurement techniques as the hot wire method, and are an established scientific field of research in their own respect [10-24].

It is the interest of this investigation to further the simulation tools and methods of current researchers in the solar cavity receiver community, but also take a more holistic, balanced thermal-fluid engineering approach to this exciting problem. A simpler theoretical architecture that models the convective and radiative exchange within the cavity receiver, focusing on the dynamics of the inner design module, will allow accurate simulation results to be generated faster and also allow relatively easier interpretation of the results for scientists, engineers, designers, and manufacturers interested in furthering direction in solar energy research, innovation, and implementation.

In the following section, the objective of the investigation and the methodology of analysis will be described. The reader should be careful to note the unique, yet relatively simple architecture of the analysis in comparison to the more complicated studies described above.

6

Chapter 3. Objective of Investigation and Methodology of Analysis

Objective

The objective of this study is to develop a simulation method and tool for the characterization of the radiative and convective heat transfer behavior of a solar cavity receiver.

The objectives of the simulation method and tool are four-fold:

1) Accurately model the steady state heat transfer, convective and radiative exchange, between surfaces in the system

2) Optimize the geometric size and spatial conformation of the system, to maximize heat transfer into the working fluid

3) Support current experimental results in solar energy design based literature findings

4) Translate the optimized steady state model into a transient model for simulation, design, development, and testing purposes of an actual solar cavity receiver

The preliminary objective and the purpose of this investigation, is to develop a simulation tool that can translate the steady state thermal analysis of the system into corresponding optimization of geometric orientation and working conditions for the capture, collection of solar thermal energy power.

Geometry of Interest

In order to develop a simulation tool for the thermal and heat transfer characterization of a solar cavity receiver system, it is imperative that the geometric conformation and spatial orientation of the system is first taken into respect.

A solar cavity receiver system as shown in Figures 1 and 2, typically has 4 main parts

1) The aperture or the small opening for the entry of solar radiation

2) The encasing metallic ring of the aperture (simulated as a flat plate)

3) Metallic helical coils which circumvent the cavity system shape

7

4) A polished metallic reflector at the bottom of the system (simulated as a flat plate)
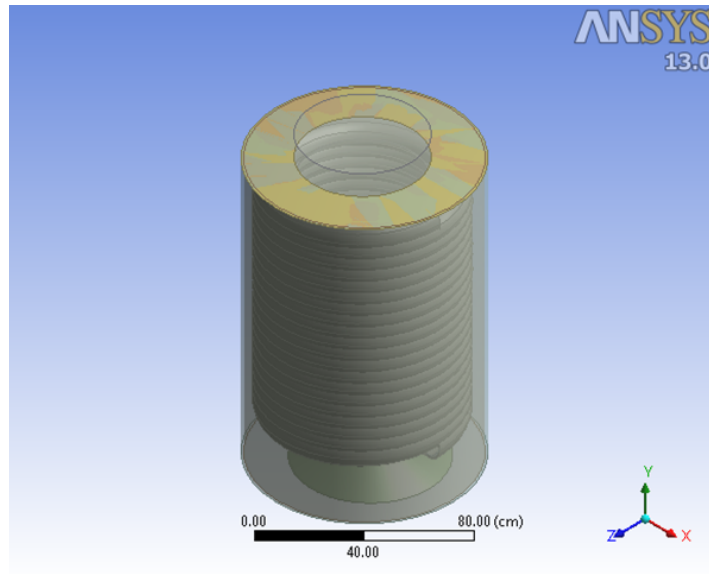
Fig.1. Schematic of a solar cavity receiver (front view)
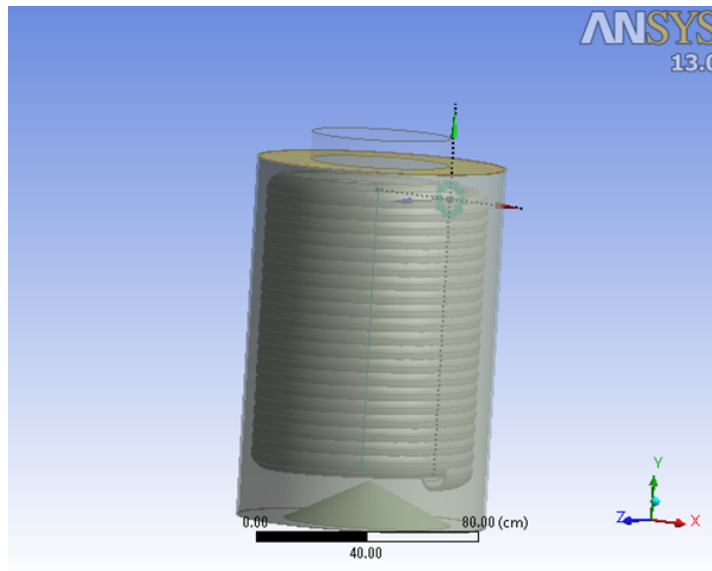
Fig.2. Schematic of a solar cavity receiver (side view)

The first part of the solar cavity receiver, the aperture, serves an opening to allow incoming, concentrated solar heat flux from the point concentrators into the cavity receiver system. The aperture's diameter plays a crucial role how the solar flux is distributed throughout the system. The second part of the solar cavity system, the

encasing metallic ring of the aperture, is one that forms the solid surface of the top of the cavity system. This ring is usually insulated.

The metallic helical coils that circumvent the cavity system shape, in this case cylindrical, are the most crucial part of the system. These coils contain working fluid, typically a molten salt or other heat exchanger fluid, which flow at varied rates, hence have varying Reynolds numbers and heat convention coefficients. In optimizing the geometric nature and spatial properties of these coils, working fluid energy gains and losses, hence power generation, within the entire system are optimized. Lastly the reflector of the cavity system serves a means to re-distribute any heat not already absorbed by the working fluid, back to the working fluid to maximize energy gains.

Developing a Theoretical Model

In order to analytically and numerically model such geometry with dynamic fluid and heat transfer changes, the cavity receiver system (Figs. 1-2), is divided into a simpler, labeled parts. For initial steady state purposes, the solar cavity receiver is modeled as in Figure 3.
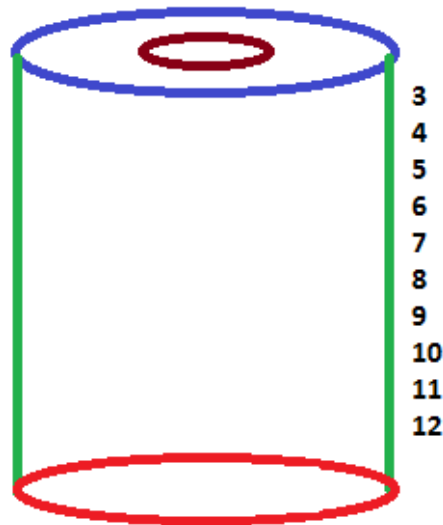
Fig.3. Geometry for cavity receiver system with aperture, surface 2 (the aperture through which solar energy enters), lid or surface 1 (top circle), inner helical coil or surfaces 3-12 (side wall), and reflector or surface 13 (bottom circle).

Figure 3 schematically represents a typical solar cavity receiver system in Figures 1-2, where the wall surface (surfaces 3-12) represents the interior of the helical coils. It is our basic assumption based on the conservation of energy that the radiative heat flux incoming to the system, will be mostly transferred to the coils and the heat transfer fluid in the coil at the interior of the coils.

In the case of the cavity receiver, there are numerous instances of multi-mode heat transfer. It was the initial goal to model the radiative heat transfer phenomena accurately, specifically focusing on the surface-to-surface heat exchange in the cavity system. The incoming heat flux into the aperture will quickly raise the temperature of the aperture; hence initiate a series of heat transfer exchanges amongst the surfaces in the cavity system enclosure.

Surface to surface heat exchange in a gray enclosure is defined by assuming each surface within the enclosure to be isothermal, hence characterized by a uniform radiosity and irradiation [25]. Furthermore the medium within the enclosure is taken to be nonparticipating. It is by the net radiative flux, q_i, that the associated temperature of the surface is determined [25].

Applying an energy balance to any arbitrary surface in an enclosure, as the aperture in the cavity receiver system, the net rate at which radiation leaves the surface, is equal to the difference between the surface radiosity and irradiation (1),[25].

$$q_i = A_i * (J_i - G_i) \tag{1}$$

$$J_i = E_i + \rho_i * G_i \tag{2}$$

Plugging equation (2) into equation (1) and utilizing $\rho_i = 1 - \epsilon_i$,
results in equation (3).

$$q_i = (Eb_i - J_i) * \left(\frac{\varepsilon_i * A_i}{1 - \varepsilon_i}\right) \tag{3}$$

Where q_i is the net radiative flux of the surface, A_i is the area of the surface, J_i is the incoming radiative flux of the surface, G_i is the outgoing radiative flux of the surface, E_i is the emissive power of the surface, ϵ_i is the emissivity of the surface, and ρ_i is the reflectivity of the surface.

Equation (3) gives a net radiative heat transfer rate from the surface given the known temperature values, as relation to the black body emissive power of the surface, Eb_i, and the outgoing radioisities of the surfaces, J_i [25].

Utilizing the concept of a view factor [25], which geometrically links the fraction of the radiation leaving an arbitrary surface and intercepted by a neighboring surface (4-6), we can relate incoming heat fluxes to an arbitrary surface from exchanges with neighboring surfaces in the same enclosure (7-9).

$$F_{ij} = \frac{1}{A_i} * \frac{\int_{Ai} \int_{Aj} \cos(\theta_i) * \cos(\theta_j)}{\pi * R^2} * dA_i * dA_j \tag{4}$$

$$A_i * F_{ij} = A_j * F_{ji} \tag{5}$$

$$\sum_{j=1}^{N} F_{ij} = 1 \tag{6}$$

$$A_i * G_i = \sum_{j=1}^{N} A_i * F_{ij} * J_j \tag{7}$$

Where F_{ij} is the view relationship between surfaces, θ_i and θ_j are the angles of orientations of the surfaces, and R is the distance between the surfaces.
Utilizing equations (1, 5-6) and reducing equation (7) results in equation (8).

$$q_i = A_i * \left(\sum_{j=1}^{N} F_{ij} * J_i - \sum_{j=1}^{N} F_{ij} * J_j \right) \tag{8}$$

Equating equation (3) to equation (8) results in equation (9).

$$q_i = (Eb_i - J_i) * \left(\frac{\varepsilon_i * A_i}{1 - \varepsilon_i}\right) = \sum_{j=1}^{N} \frac{J_i - J_j}{\left(A_i * F_{ij}\right)^{-1}} \qquad (9)$$

As the case with different spatial orientations of geometry, the view factor relationships change and values behave according to the defined view factor relationship expression. For the purposes of this study, all view factor relationships and sample calculations used are included in Appendix A.

It is from equation (9), that we receive the net radiative heat transfer rate at an arbitrary surface, given known temperatures and emissivities of surfaces, and view factor relationships amongst surfaces.

As explained earlier, in gray enclosures, all surfaces are isothermal, and hence have a constant temperature once thermal equilibrium is obtained. It is logical to assume at a given surface, the net energy balance should be zero, as to maintain that constant temperature of the surface, amongst interactions with other surfaces and losses/gains by conduction and convention.

As in the case of Figure 3, net energy balances must equate to zero for all surfaces in order to complete the initial objective of identifying changes in thermal dynamics within the cavity system. The energy balances for Figure 3 are given by equations (10-12), utilizing equation (9) as the basis of the radiative exchanges between surfaces.

Energy Balance for Reflector and Lid

$$q_k = 0 = \sigma * \sum_{j=1}^{13} \frac{T_j^4 - T_k^4}{\frac{1-\varepsilon_j}{\varepsilon_j * A_j} + \frac{1}{A_k * F_{kj}} + \frac{1-\varepsilon_k}{\varepsilon_k * A_k}} - \frac{(kf_k * (T_k - T_\infty) * A_k)}{t} \tag{10}$$

Where k=1,13

Energy Balance for Aperture

$$q_2 = 0 = \sigma * \sum_{j=1}^{13} \frac{T_j^4 - T_2^4}{\frac{1-\varepsilon_j}{\varepsilon_j * A_j} + \frac{1}{A_2 * F_{2j}} + \frac{1-\varepsilon_2}{\varepsilon_2 * A_2}} - (h_2 * A_2 * (T_2 - T_\infty)) + qsolar \tag{11}$$

Energy Balance for Helical Coils

$$q_i = 0 = \sigma * \sum_{j=1}^{13} \frac{T_j^4 - T_i^4}{\frac{1-\varepsilon_j}{\varepsilon_j * A_j} + \frac{1}{A_i * F_{ij}} + \frac{1-\varepsilon_i}{\varepsilon_i * A_i}} - hf_i * A_i * (T_i - T_{mi}) \tag{12}$$

Where i=3 to 12, $T_{mi} = \frac{1}{2} * (Tfo_i + Tfi_i)$

Where T_j and T_k are temperatures of the surfaces, T_m is the mean temperature of the fluid, kf_k is the thermal conductivity of the surface, h_2 is the heat convection coefficient of the aperture, qsolar is the incoming solar flux, Tfo_i is the outlet fluid temperature, Tfi_i is the inlet fluid temperature, and σ is the Stefan-Boltzmann constant.

As explained earlier, at the top of the cavity system, the metallic lid is insulated (10) and the aperture experiences both convective losses to the atmosphere and heat gains from the incoming solar flux, qsolar, which is arbitrary for initial purposes (11). At the wall sections of the helical coil, there is convection from working fluid flow with radiative heat transfer solely reliant on exchanges with the neighboring surfaces in the enclosure (12). The heat convention coefficient, hf_i, for the working fluid in the helical coil is calculated using the following procedure (13-19).

$$\dot{m} = \rho * v * \frac{di^2}{4} * \pi \tag{13}$$

13

$$Re_D = \frac{\rho * v * di}{\mu} \tag{14}$$

$$Pr = cp * \frac{\mu}{k} \tag{15}$$

$$Re_{critical} = 2100 * (1 + 12 * \delta^{0.5}) \tag{16}$$

If $Re_D < Re_{critical}$

$$Nu_D = 3.65 + 0.08 * [1 + 0.8 * \delta^{0.9}] * Pr^{\frac{1}{3}} * Re_D^m \tag{17}$$

where $m = 0.5 + 0.2903 * \delta^{0.194}$

If $Re_D > Re_{critical}$

$$Nu_D = 0.023 * Re_D^{0.85} * Pr^{0.4} * \delta^{0.1} \tag{18}$$

$$hf_i = Nu_D * \frac{k}{di} \tag{19}$$

Given the mass flow rate, $\dot{m}$, as designated by the velocity flow choice, v, the Reynolds number, Re_D, is calculated using di, the diameter of the pipe, density of fluid, ρ, and viscosity of fluid, μ (13-14) and subsequently the Prandtl number, Pr, can be calculated utilizing cp, specific heat of the fluid (15). Utilizing the well known relationship, as mathematically described by Srvinvasan in 1968 [16], the critical Reynolds number, $Re_{critical}$, for the transition from laminar to turbulent flow, can be calculated via equation (16), where δ is the ratio of diameter of helical coil to diameter of the coil pipe. If the Reynolds number, is less than that of the critical Reynolds number, then the Nusselt number, Nu_D, for laminar flow, as determined mathematically and numerically by Ling, Zhang, and Ebadian in 1996 [24], can be calculated via equation (17). If the Reynolds number is greater, the Nusselt number for the turbulent flow can be determined as described by Rogers and Mayhew [18] in 1964 by equation (18). Given laminar or turbulent flow, equation (19) is utilized to determine the heat convection coefficient, hf_i, of the working fluid, given the correct Nusselt number (17-18).

For the preliminary investigation and design of a simulation tool, incompressible flow satisfying the continuity equation, neglecting frictional, temperature dependent properties, pressure drop effects was assumed, hence the heat convection coefficient of the working fluid was constant, no matter the geometric location within coil. Utilizing this information and additional emissivities, geometrical, physical properties of surfaces, the set of non-linear equations can be solved simultaneously (10-12). The choice for the non-linear solver, was "fsolve", apart of the MATLAB software package 2011.

The non-linear equations given by equation (10-12), would not only solve for the wall temperatures of the cavity receiver system, but also the working temperatures within the cavity receiver system via equation (12). Taking into mind that the system is insulated, other than the aperture and helical coil, it is logical to assume that the majority of the solar flux input, qsolar, would be received by the helical coil pipes based on the conservation of energy. From equation (12), it can be demonstrated that

$$hf_i * A_i * (T_i - T_{mi}) = \dot{m} * cp * (Tfo_i - Tfi_i) \qquad (20)$$
$$\text{where i=3 to 12, } T_{mi} = \frac{1}{2} * (Tfo_i + Tfi_i)$$

the energy gained and retained by the flow in the helical pipe will equal the convective energy loss to the atmosphere, as a result of the convective nature of flow (20). This in return should equal the solar input, qsolar, into the system.

It is imperative to understand that this theoretical framework forms the backbone of the present simulation model and the relative measure of its accuracy. Failure to satisfy to the equations directly disqualifies the preliminary legitimacy of the simulation tool and method.

Solution of the non-linear set equations given the correct simulation tool, will result in accurate working fluid temperature and heat flux distribution of the cavity receiver. More importantly the temperature and heat flux distribution with the helical coils can relay analysis into the potential design and optimization of solar cavity

receivers. Finally these distributions can be lead to analysis of the energy generated, E_{gen} (21) and efficiency of the system, $\in$ (22).

$$E_{gen}\dot{} = \dot{m} * cp * (Tfo_i - Tfi_i) \tag{21}$$

$$\in = \left(\frac{E_{gen}}{qsolar}\right) * 100\% \tag{22}$$

Specifications of the Theoretical Model

For the interest of this study, the working fluid temperature used is Solar Salt [26], the heat transfer fluid of 60% $NaNO_3$, 40% KNO_3 composition with physical properties as defined in Table 1.

Table 1. Working heat transfer fluid properties for Solar Salt, 60% $NaNO_3$, 40% KNO_3

Melting point (K)	Specific Heat @ 400 C (J/(kg*K)	Density @ 400 C (kg/m³)	Viscosity @ 400 C (Pa*s)	Thermal Conductivity @ 400 C (W/(m*K))
495	2,660	1,840	0.0017	0.55

It was of the interest to study the effects of changes in geometry in the cavity receiver system on the working fluid temperature and heat flux distribution. As previously described, changes in the geometric properties of components in the system, will directly influence the thermal dynamics and outcome of the cavity system.

For the purpose of this study, several cases, cases A through I (Tables 3-5), were chosen in relation to changes in geometry of the cavity receiver length, aperture diameter, and helical coil pipe diameter. The dimensionless parameters of cases A through I are as defined as in Table 2.

Table 2. Cavity receiver geometric dimensionless variables and definitions

Dimensionless variables	Physical Definition	Symbolic Definition
1	Ratio of Length of Cavity Receiver to Length of Helical Coil	L/Lc
h	Ratio of Length of Cavity Receiver to Diameter of Cavity Receiver	L/Dc
a	Ratio of Diameter of Cavity Receiver to Diameter of Aperture	Dc/Da
b	Ratio of Diameter of Cavity Receiver to Diameter of Helical Coil	Dc/Do
c	Ratio of Diameter of Helical Coil to Diameter of Aperture	Do/Da
e	Ratio of Length of Cavity Receiver to Diameter of Aperture	L/Da
δ	Ratio of Diameter of Helical Coil to Diameter of Coil Pipe	di/Do
N	Ratio of Length of Helical Coil to Diameter of Helical Pipe	Lc/di

Table 3. Case A, B, and C for changing length of cavity receiver

Case	Description	l	h	a	b	c	e	δ	N
A	Tightly Packed (L=110 cm)	**1.1**	**1.4**	8.0	1.0	8.0	**11.0**	0.015	83.0
B	Medium Packed (L=150 cm)	**1.5**	**1.9**	8.0	1.0	8.0	**15.0**	0.015	83.0
C	Loosely Packed (L=200 cm)	**2**	**2.5**	8.0	1.0	8.0	**20.0**	0.015	83.0

Table 4. Case D, E, and F for changing diameter of aperture

Case	Description	l	h	**a**	b	**c**	e	δ	N
D	Small Gap (Da=10 cm)	1.1	1.4	**8.0**	1.0	**8.0**	**11.0**	0.015	83.0
E	Medium Gap (Da=20 cm)	1.1	1.4	**4.0**	1.0	**4.0**	**5.5**	0.015	83.0
F	Large Gap (Da=60 cm)	1.1	1.4	**1.3**	1.0	**1.3**	**1.8**	0.015	83.0

Table 5. Case G, H, and I for changing diameter of helical coil

Case	Description	l	h	a	b	c	e	**δ**	**N**
G	Small Pipe (di=12 mm)	1.1	1.4	8.0	1.0	8.0	11.0	**0.015**	**83.0**
H	Medium Pipe (di=20 mm)	1.1	1.4	8.0	1.0	8.0	11.0	**0.025**	**50.0**
I	Large Pipe (di=40 mm)	1.1	1.4	8.0	1.0	8.0	11.0	**0.050**	**25.0**

Each of the cases A through I listed in Tables 3 to 5 represents the parametric variations in length and diameter of the cavity receiver as well as diameter of the aperture. These are evaluated for 3 different inlet flow velocities and 3 different solar fluxes, resulting in 81 different cases simulated to further understand the effects of various parameters on the thermal behavior leading to an optimal design of the solar cavity receiver system. These 81 different cases are described in Appendix B. For all simulation cases, it is assumed that the emissivity properties of the system are as given in Table 6.

Table 6. Emissivities of surfaces

System Component	Surface	ε
Aperture	2	1.00
Lid	1	0.90
Reflector	13	0.10
Helical Coil Wall	3-12	0.95

Areas of the surfaces can be calculated, using equations (23-26).

Area of Lid

$$\pi * \left(\frac{Dc^2}{4}\right) - \pi * (\frac{Da^2}{4}) \quad (23)$$

Area of Aperture

$$\pi * (\frac{Da^2}{4}) \quad (24)$$

Area of Reflector

$$\pi * \left(\left(\frac{Dr}{2}\right) * \left(\frac{\left(\frac{Dr}{2}\right)}{\cos(\theta)}\right) + \pi * \left(\frac{Dr}{2}\right)^2 \quad (25)\right.$$

Area of Helical Coil

$$\frac{(\pi * Dr * di) * \left(\frac{Lc}{di}\right)}{10} \quad (26)$$

Where Dc is the diameter of the cavity receiver, Da is the diameter of the aperture, Dr is the diameter of the reflector, Lc is the length of cavity receiver, and di is the diameter of the pipe. Finally for all simulation cases, the following properties are assumed for initial purposes.

Table 7. Properties of solar cavity receiver

T_∞	273 K
T_{inlet}	350 K
h_2	20 W/(m^2*K),
kf	0.09 W/(m*K)
t	1,000 mm

Where T_∞ is the outside air temperature, T_{inlet} is the inlet fluid temperature, h_2 is the heat convection coefficient of the aperture, and t is the thickness of the cavity receiver wall insulation.

In conclusion, the objective of the investigation and the methodology of analysis have been presented. The analysis presented is relatively simple in its theoretical nature, but provides a way to quantify and characterize the thermal dynamics of the cavity receiver. In the following section, the results and discussion will be presented for the simulation test cases (Appendix B).

Chapter 4. Results &Discussion

The objective of this study was to develop a simulation method and with a parametric study a tool for the characterization of the thermal and heat transfer behavior of a solar cavity receiver. In accordance with the initial objective of the development of a simulation tool and method, the set of non-linear equations (10-12) were solved for the cases A through C given in Tables 3 to 5.

Effect of Cavity Receiver Length on Thermal Dynamics of System

The first parameter considered for study is the effect of the cavity receiver length on the thermal dynamics of the cavity receiver. The results of these findings would provide an initial point to complete the first two of four objectives in this investigation.

The non-linear solutions to the set of equations for an inlet velocity of 0.1 m/s and solar input of 1 kW, for case A through C, demonstrated a more rapid and stronger increase in working fluid temperature for case A, referring to the tightly packed system than case B and C, medium and loosely packed systems respectively (Table 3), across fractional depth into the cavity receiver (Fig. 4).
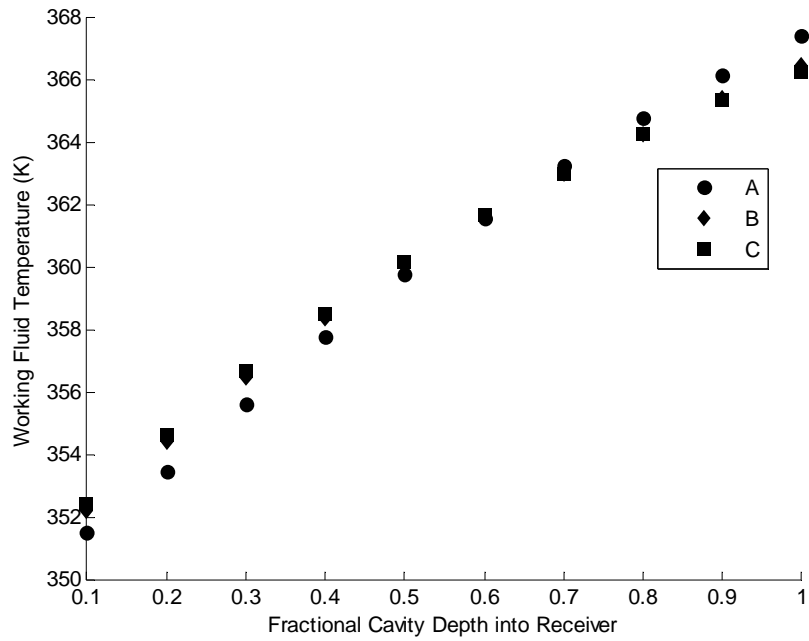
Fig.4. Effect of coil packing in cavity receiver on working fluid temperature for case A,B, and C (l=1.1, 1.5, and 2) for inlet velocity of 0.1 m/s, qsolar of 1 kW, laminar Reynolds number of 1,300, and heat convection coefficient of 850 W/(m^2*K).

An energy balance given the temperature values as solved for in Figure 4, was conducted according to relationships for surfaces in equation (10-12). A quick check of the energy balance for the solution yields the accuracy of this model (Fig. 5).
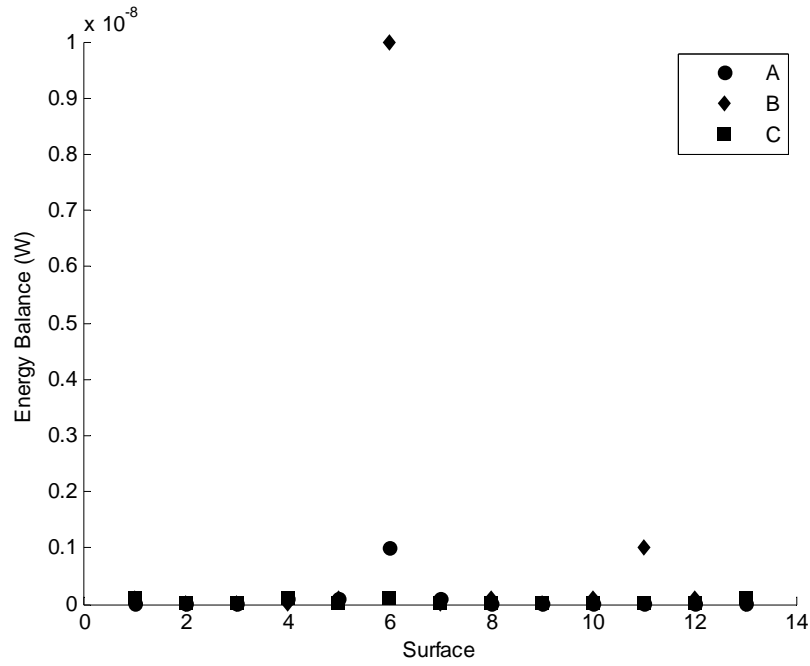
22

Fig.5. Energy balance for solution of case A,B, and C (l=1.1, 1.5, and 2) for inlet velocity of 0.1 m/s, qsolar of 1 kW, laminar Reynolds number of 1,300, and heat convection coefficient of 850 W/(m^2*K).

     As the solar input, increased from 1 kW to 10 kW, similar behavior was noticed, but at higher temperatures (Fig. 6).
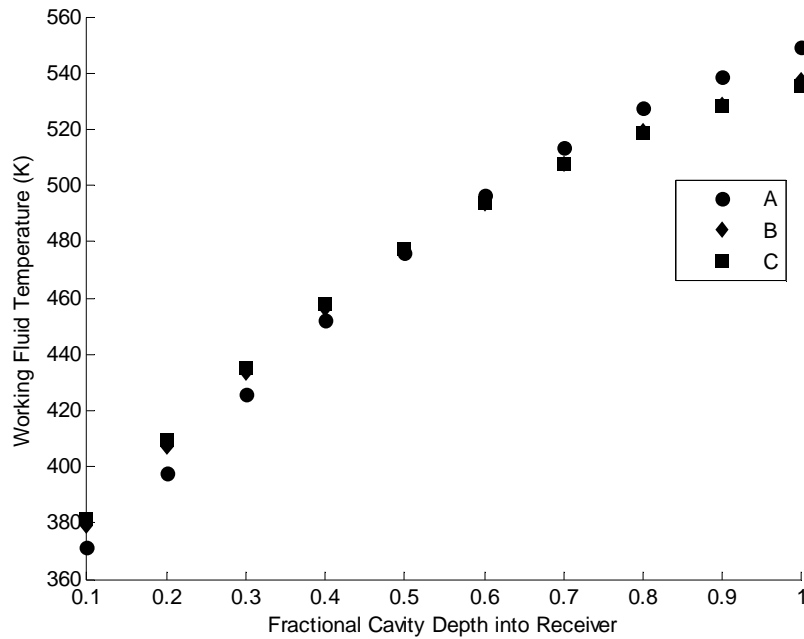
Fig.6. Effect of coil packing in cavity receiver on working fluid temperature for case A,B, and C (l=1.1, 1.5, and 2) for inlet velocity of 0.1 m/s, qsolar of 10 kW, laminar Reynolds number of 1,300, and heat convection coefficient of 850 W/(m^2*K).

As qsolar is increased 1 to 10 kW, for laminar flow, 0.1 m/s, Reynolds number of 1,300, the final outlet temperature increased from 367 K to 550 K (Fig. 4,6). Case A experiences more rapid and stronger working fluid temperature across fractional cavity depth into receiver, than cases B and C, which experience similar increases in working fluid temperature (Figs. 4,6).

As inlet velocity, increased to 1 m/s, Reynolds number of 13,000, smaller increases in working fluid temperature across fractional cavity depth into receiver for case A through C was observed for both 1 and 10 kW (Figs. 7, 8). It is observed that for the 1 and 10 kW solar input, the difference between the inlet and outlet temperature is a 10-fold decrease going from laminar to turbulent flow (Figs. 4, 6, 7, and 8).
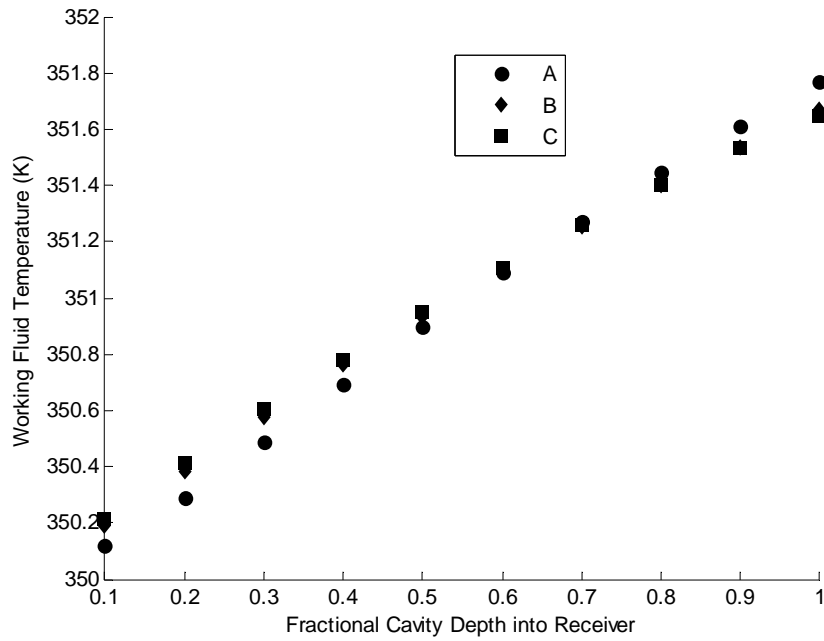
Fig.7. Effect of coil packing in cavity receiver on working fluid temperature for case A,B, and C (l=1.1, 1.5, and 2) for inlet velocity of 1 m/s, qsolar of 1 kW, turbulent Reynolds number of 13,000, and heat convection coefficient of 5,050 W/(m^2*K).

Fig.8. Effect of coil packing in cavity receiver on working fluid temperature for case A,B, and C (l=1.1, 1.5, and 2) for inlet velocity of 1 m/s, qsolar of 10 kW, turbulent Reynolds number of 13,000, and heat convection coefficient of 5,050 W/(m^2*K).

Further investigation into the heat flux distribution for the coil, demonstrated that as the inlet velocity increased from 0.1 to 1 m/s, Reynolds number from 1,300 to 13,000, cases A, B exhibited a net heat transfer distribution with a local maximum, with the maximum net heat transfer rate occurring around 0.3-0.4 and 0.1 of the fractional cavity depth into the receiver respectfully, while case C, which relates to a loosely packed system or one in which "l" is 2, exhibited a linear decrease in net heat transfer rate with increasing cavity depth (Figs. 9, 10, 11, and 12).
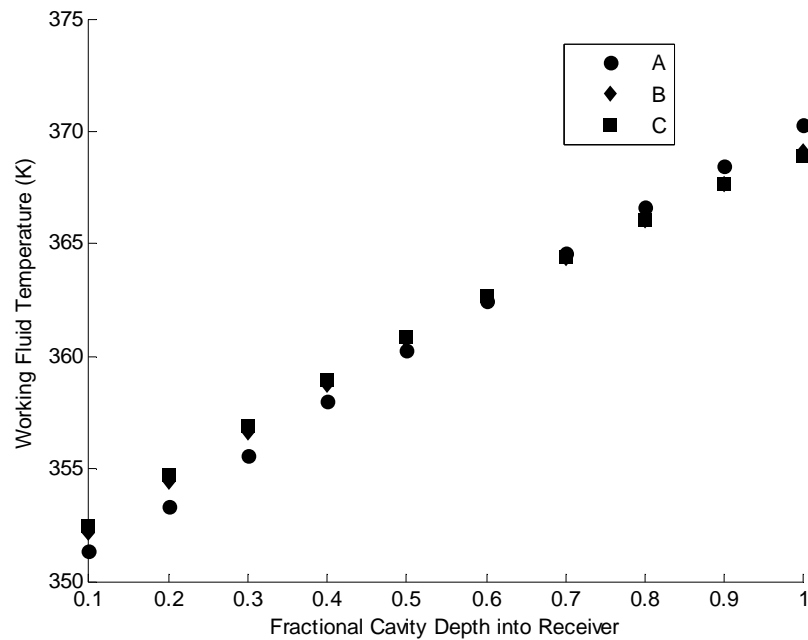

Fig.9. Effect of coil packing in cavity receiver on working fluid temperature for case A,B, and C (l=1.1, 1.5, and 2) for inlet velocity of 0.1 m/s, qsolar of 1 kW, laminar Reynolds number of 1,300, and heat convection coefficient of 850 W/(m^2*K).
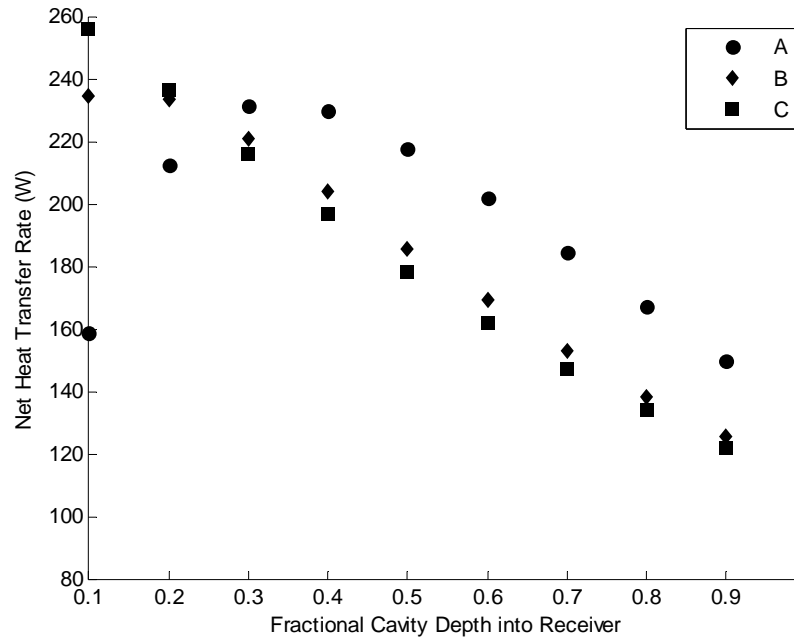
Fig.10. Effect of coil packing in cavity receiver on working fluid temperature for case A,B, and C (l=1.1, 1.5, and 2) for inlet velocity of 0.1 m/s, qsolar of 10 kW, laminar Reynolds number of 1,300, and heat convection coefficient of 850 W/(m^2*K).

Fig.11. Effect of coil packing in cavity receiver on net heat transfer rate for case A, B, and C (l=1.1, 1.5, and 2) for inlet velocity of 1 m/s, qsolar of 1 kW, turbulent Reynolds number of 13,000, and heat convection coefficient of 5,050 W/(m^2*K).
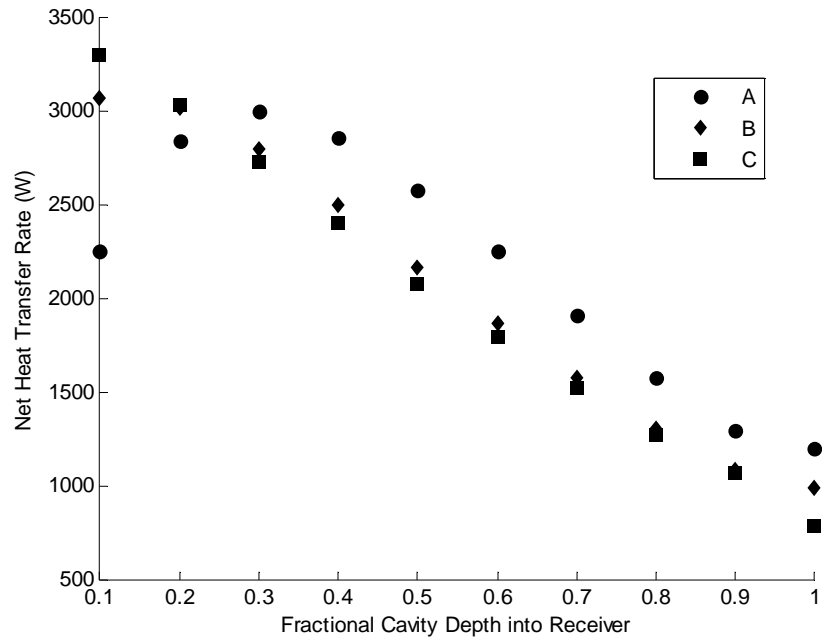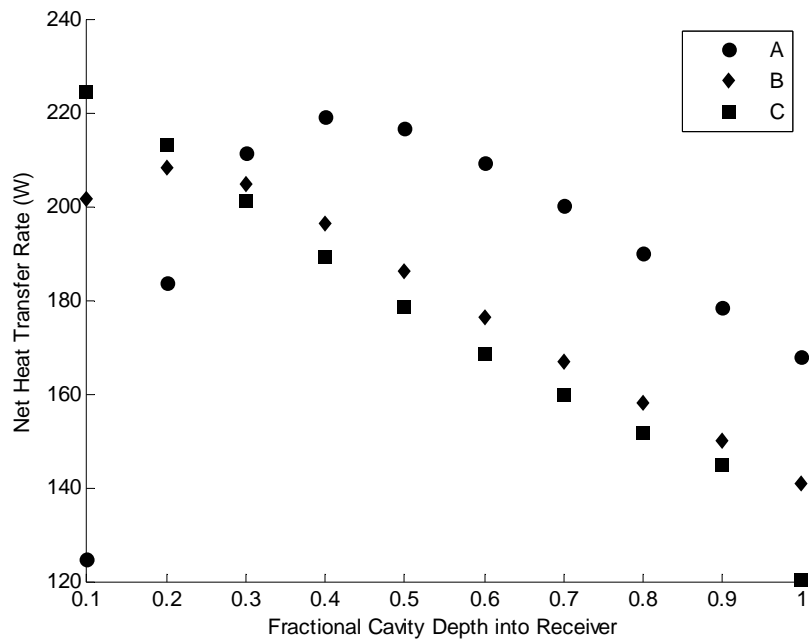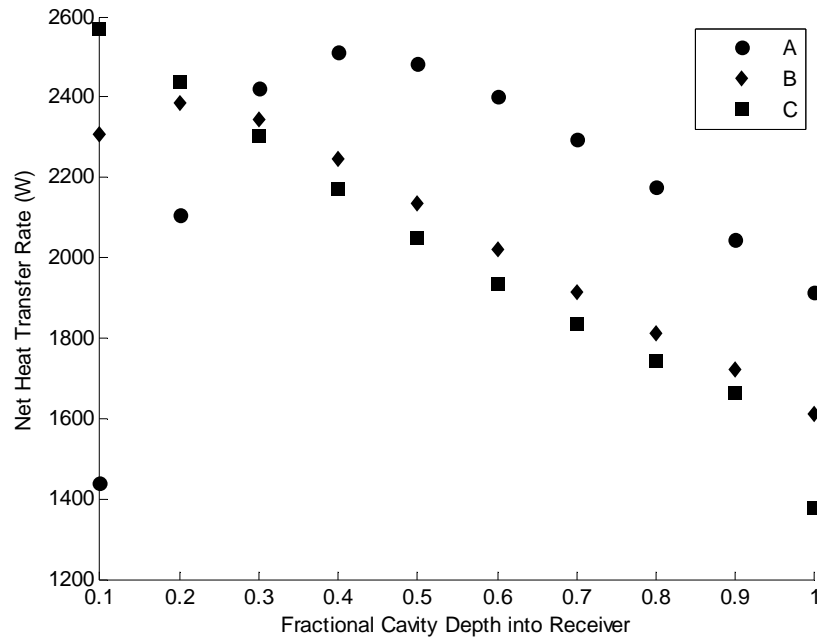
27

Fig.12. Effect of coil packing in cavity receiver on net heat transfer rate for case A,B, and C (l=1.1, 1.5, and 2) for inlet velocity of 1 m/s, qsolar of 10 kW, turbulent Reynolds number of 13,000, and heat convection coefficient of 5,050 W/(m^2*K).

Intuitively, as the length of the cavity receiver increases, as in case C, the view factor relationship between the aperture and the neighboring surfaces decreases, hence radiative exchange of the incoming solar flux from the aperture to the other surfaces is weaker than in cases A and B, which are more tightly compacted systems. As a result, weaker view factor distributions for the middle and bottom of the cavity receiver, do not receive as much radiation as the top of cavity receiver (Figs. 9-12).

In contrast to case C, where the system is loosely packed, view factor relationships for tightly packed systems as cases A and B, in the mid-section of the helical coil are stronger from influences from the aperture and top, bottom sections of the helical coil. This in return correlates to stronger and more rapid increases in working fluid temperature in the midsection of the coil and overall higher working fluid temperatures for tightly packed systems (Figs. 4, 6, 7, and 8).

From these simulation results, it can be observed that this model firstly abides by the basic, intuitive theoretical architecture, by having energy balances of the system

28

equate to zero as demonstrated in Figure 5. Further the results provide initial understanding of the thermal dynamics of the system, given varying flow velocities and solar inputs.

It is finally concluded from this analysis, that a more tightly packed system, case A, provides higher working fluid temperatures and heat transfer distributions, given varied flow rates and solar inputs.

Effect of Aperture Diameter on Thermal Dynamics and Losses of System

With initial confidence in the simulation tool, attention was turned to the understanding of the aperture and its relative size. As described in the Table 4, case D, E, and F correspond to varying aperture sizes, 10-60 cm, with dimensionless values for a and c of 8, 4, and 1.3 respectively.

It was observed, for both solar inputs of 1 and 10 kW with flows of Reynolds number of 1,300 and 13,000 and heat convection coefficient of 850 and 5,050 W/(m^2*K) respectively, the larger the cavity receiver to aperture diameter ratio, "a", as in the case of D, the stronger and more rapid increases in working fluid temperature in comparison to cases as E and F, with smaller, "a" ratios, 4.0 and 1.3 respectively (Figs. 13-16).

Fig.13. Effect of aperture diameter on working fluid temperature for case D, E, and F (a and c=8,4, and 1.3), for inlet velocity of 0.1 m/s, qsolar of 1 kW, laminar Reynolds number of 1,300, and heat convection coefficient of 850 W/(m^2*K).

Fig.14. Effect of aperture diameter on working fluid temperature for case D, E, and F (a and c=8,4, and 1.3), for inlet velocity of 0.1 m/s, qsolar of 10 kW, laminar Reynolds number of 1,300, and heat convection coefficient of 850 W/(m^2*K).

Fig.15. Effect of aperture diameter on working fluid temperature for case D, E, and F (a and c=8,4, and 1.3), for inlet velocity of 1 m/s, qsolar of 1 kW, turbulent Reynolds number of 13,000, and heat convection coefficient of 5,050 W/(m²*K).
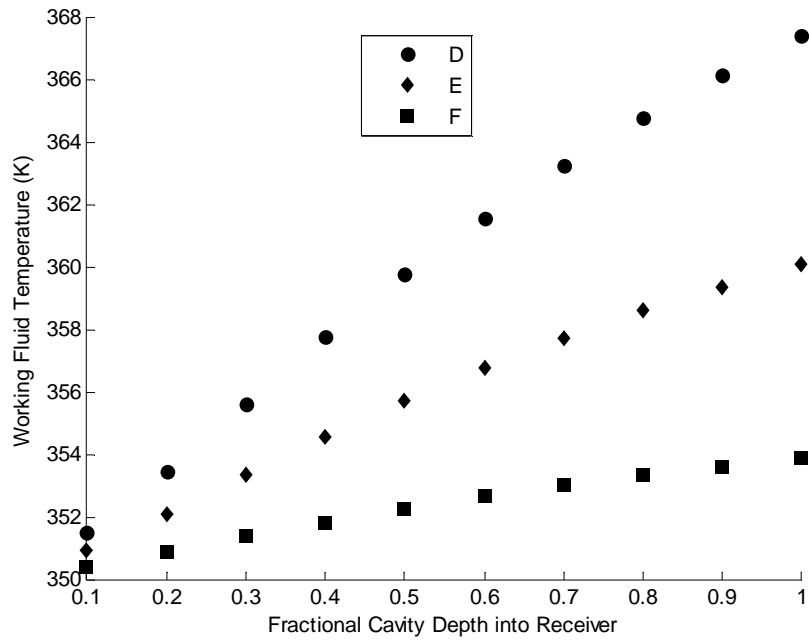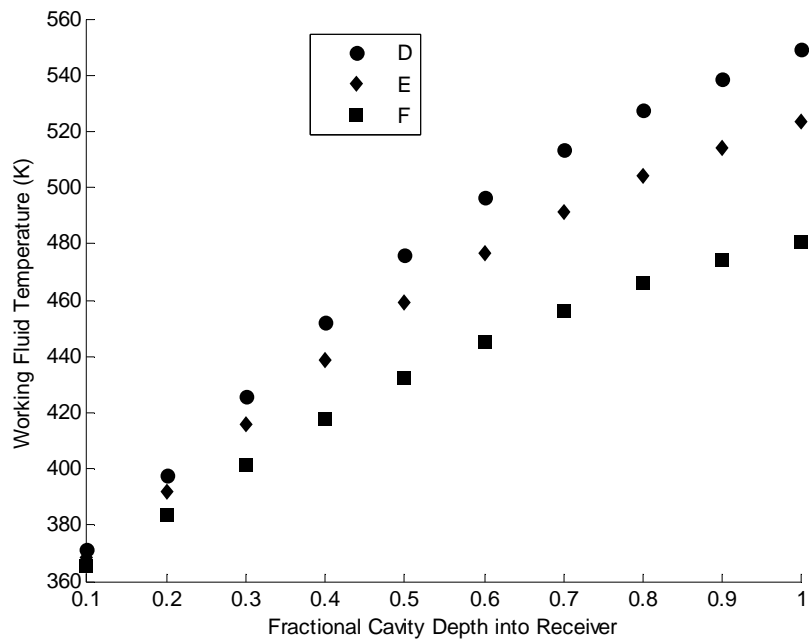

Fig.16. Effect of aperture diameter on working fluid temperature for case D, E, and F (a and c =8,4, and 1.3), for inlet velocity of 1 m/s, qsolar of 10 kW, turbulent Reynolds number of 13,000, and heat convection coefficient of 5,050 W/(m²*K).

Noticeably these rapid and strong increases in working fluid temperature are more noticeable in laminar flow (Figs. 13-14) than turbulent flow (Figs. 15-16).

Further investigation into the net transfer rate across the helical coil, demonstrated that case D exhibited a net heat transfer distribution with the highest local maximum in comparison to cases E and F, with maximum net heat transfer rate occurring at fractional cavity receiver depth of 0.3-0.4 (Figs. 17-20).

Fig.17. Effect of aperture diameter on net heat transfer rate for case D, E, and F (a and c =8,4, and 1.3), inlet velocity of 0.1 m/s, qsolar of 1 kW, laminar Reynolds number of 1,300, and heat convection coefficient of 850 W/(m^2*K).

Fig.18. Effect of aperture diameter on net heat transfer rate for case D, E, and F (a and c =8,4, and 1.3), for inlet velocity of 0.1 m/s, qsolar of 10 kW, laminar Reynolds number of 1,300, and heat convection coefficient of 850 W/(m^2*K).
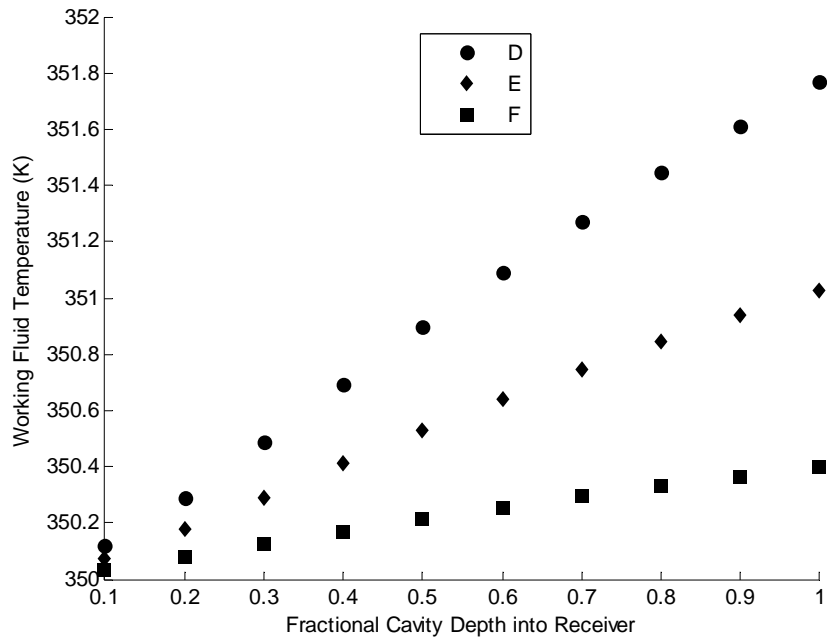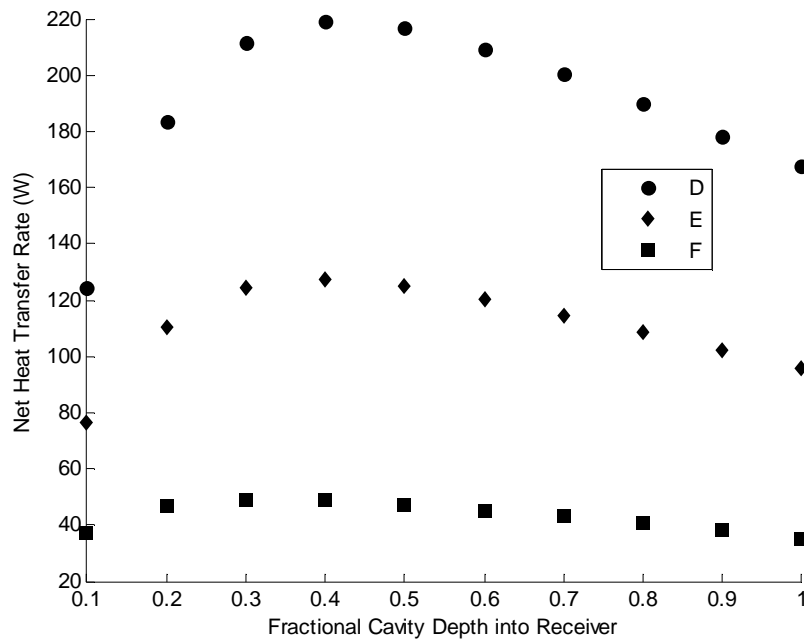

Fig.19. Effect of aperture diameter on net heat transfer rate for case D, E, and F (a and c =8,4, and 1.3), for inlet velocity of 1 m/s, qsolar of 1 kW, turbulent Reynolds number of 13,000, and heat convection coefficient of 5,050 W/(m^2*K).

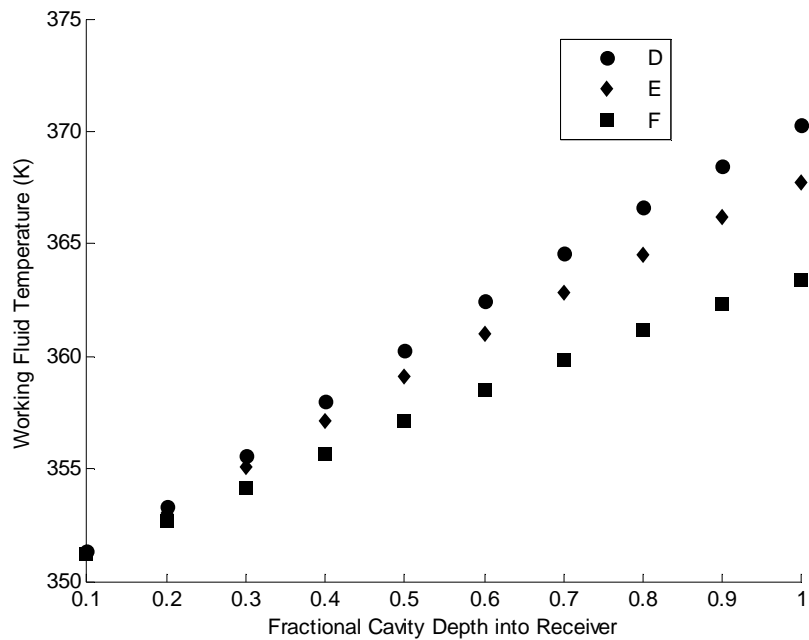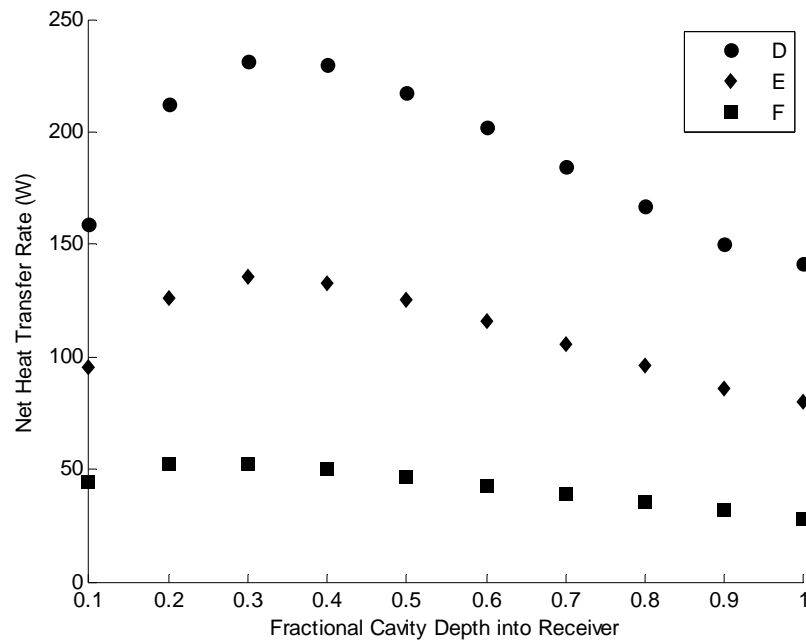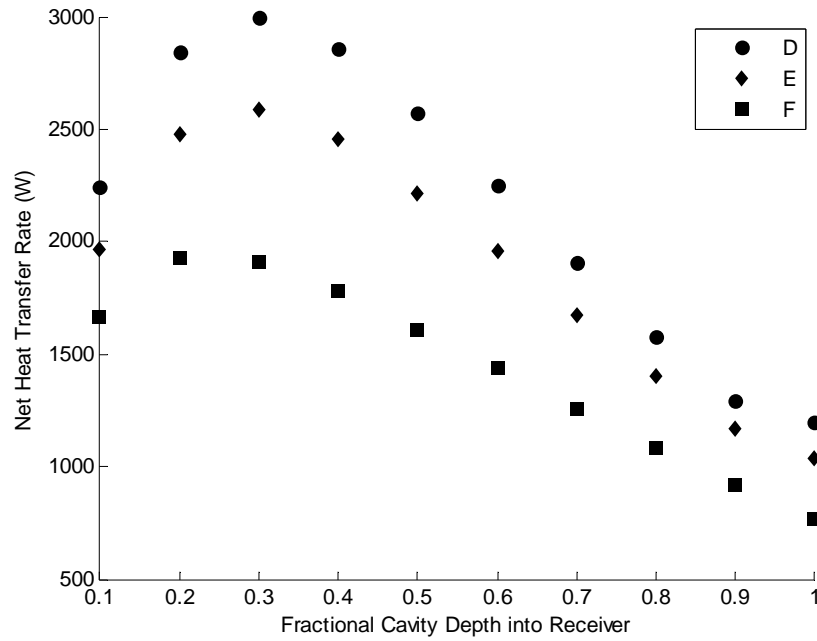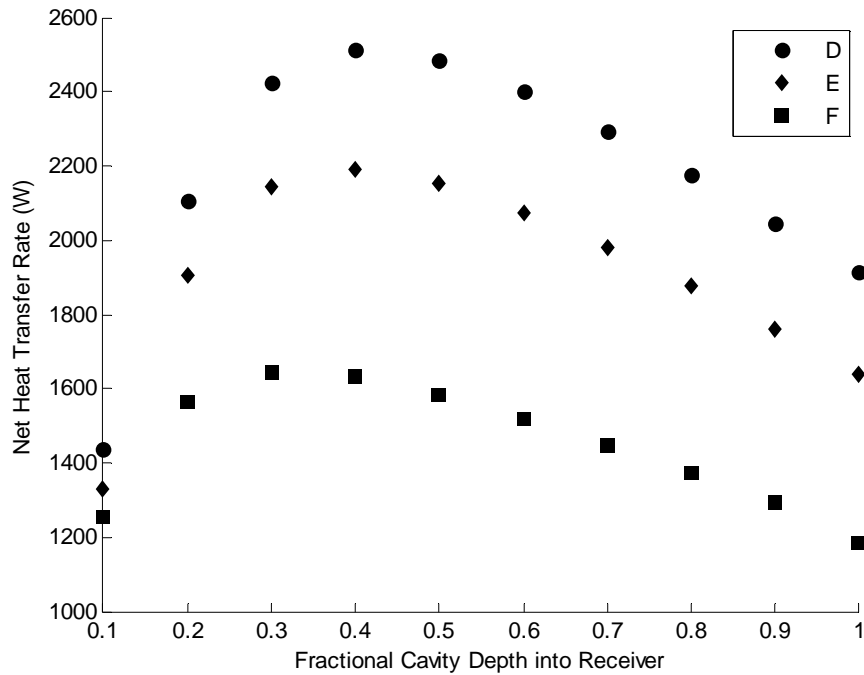**Fig.20**. Effect of aperture diameter on net heat transfer rate for case D, E, and F (a and c =8,4, and 1.3), for inlet velocity of 1 m/s, qsolar of 10 kW, turbulent Reynolds number of 13,000, and heat convection coefficient of 5,050 W/(m^2*K).

It is demonstrated that increasing the aperture size, as in case D to F, results in lower magnitudes of net heat transfer rates despite similar heat distribution behavior (Figs. 17-20). Furthermore net heat transfer rates decrease from laminar (Figs. 17-18) to turbulent (Figs. 19-20) flow for both 1 and 10 kW, corresponding to 0.0210 kg/s per kW and 0.0021 kg/s per kW for laminar flow and 0.2081 kg/s per kW and 0.02081 kg/s per kW for turbulent flow respectively.

This observation is further evidenced in studying the energy generation and efficiency of the helical coil system, as increasing the aperture size for laminar flow, results in 60-70% efficiency decrease as in the case of D to F (Table 8). Interestingly increasing solar input from 1 to 10 kW, for 0.021 kg/s per kW and 0.0021 kg/s per kW for laminar flow and 0.2081 kg/s per kW and 0.02081 kg/s per kW for turbulent flow respectively, results in not only an increase in energy generation, but also increase in efficiency (Table 8). It is demonstrated that for case E, for laminar flow, an increase

from 1 kW, 0.021 kg/s per kW, to 10 kW, 0.0021 kg/s per kW results in an increase from 56% to 97% efficiency of the system (Table 8).

Table 8. Energy input and efficiency for geometric cases D-F.

Case	kg/s per kW	a	c	E_{gen}(W)	$\in$ (%)
D		8	8	973	97
E	0.021	4	4	564	56
F		1.3	1.3	216	22
D		8	8	10,000	100
E	0.0021	4	4	9,700	97
F		1.3	1.3	7,310	73
D		8	8	979	98
E	0.2081	4	4	568	57
F		1.3	1.3	220	22
D		8	8	10,000	100
E	0.02081	4	4	9,800	98
F		1.3	1.3	7,420	74

Interestingly it noted that case D achieves close to or actually 100% efficiency (Table 8). Case D, correlates to an aperture diameter of 10 cm, with a cavity receiver diameter of 80 cm, hence it reasonable to deduce based on the theoretical architecture, that very little losses will occur at the aperture, hence all the solar input will be captured by the working fluid.

It is evident from these results, decreasing the aperture size, results in higher working fluid temperatures and net heat transfer rates as in the case D. As flow velocity increases from 0.1 to 1 m/s, 0.021 kg/s per kW and 0.0021 kg/s per kW for laminar flow and 0.2081 kg/s per kW and 0.02081 kg/s per kW for turbulent flow respectively, the working fluid temperature and net heat transfer rates decrease, as a result of flow induced convection increases, but the net transfer rate distribution behavior still remains the same whether laminar or turbulent (Figs. 13-20). Further it is interesting to observe, that increasing the solar input leads to not only increases in energy generated, but more sustainable efficiency levels, whether laminar or turbulent flow.

It is concluded based on these calculations, aperture size minimization, given a strong, sustainable solar source leads to higher energy generation and efficiency levels.

Effect of Helical Pipe Diameter on Thermal Dynamics of System

The heart of the solar cavity receiver system lies with the helical coil arrangement. As stated earlier, given the system is insulated, under conservation of energy, the coil must absorb the majority of the solar input from the aperture. The diameter of the helical pipe directly affects the flow and thermal characteristics of working fluid, hence determining how well the helical coil absorbs the majority of solar input. For purposes of this study, the diameter of helical pipe was changed from 12 to 20 to 40 mm, corresponding to case G, H, and I, with varying curvature and number turns of the helical coil (Table 5).

Fig.21. Effect of helical pipe diameter on work fluid temperature (K) through coil segment for case G,H, and I (δ=0.015, 0.025, and 0.050), for inlet velocity of 0.1 m/s, qsolar of 1 kW, laminar Reynolds number of 1,300, 2,200, and 4,300 and heat convection coefficients of 850, 733, and 650 W/(m^2*K) respectively.

Fig.22. Effect of helical pipe diameter on work fluid temperature (K) through coil segment for case G,H, and I (δ=0.015, 0.025, and 0.050), for inlet velocity of 0.1 m/s, qsolar of 10 kW, laminar Reynolds number of 1,300, 2,200, and 4,300 and heat convection coefficients of 850, 733, and 650 W/(m^2*K) respectively.

It was observed, as diameter of helical pipe increased from 12 to 40 mm, case G to I, the working fluid experienced smaller increases in temperature with increasing cavity receiver depth, for laminar flow Reynolds number of 1,300, 2,200, and 4,300 (Figs. 21-22). Interestingly as turbulent flow was onset, at the inlet velocity of 1 m/s, Reynolds number of 13,000, 22,000, and 43,000, the working fluid demonstrated similar linear behavior for temperature increases for case G-I (Figs. 23-24).

Fig.23. Effect of helical pipe diameter on work fluid temperature (K) through coil segment for case G,H,I (δ=0.015, 0.025, and 0.050), for inlet velocity of 1 m/s, qsolar of 1 kW, turbulent Reynolds number of 13,000, 22,000, and 43,000 and heat convection coefficients of 5,050, 4,900, and 4,750 W/(m^2*K) respectively.
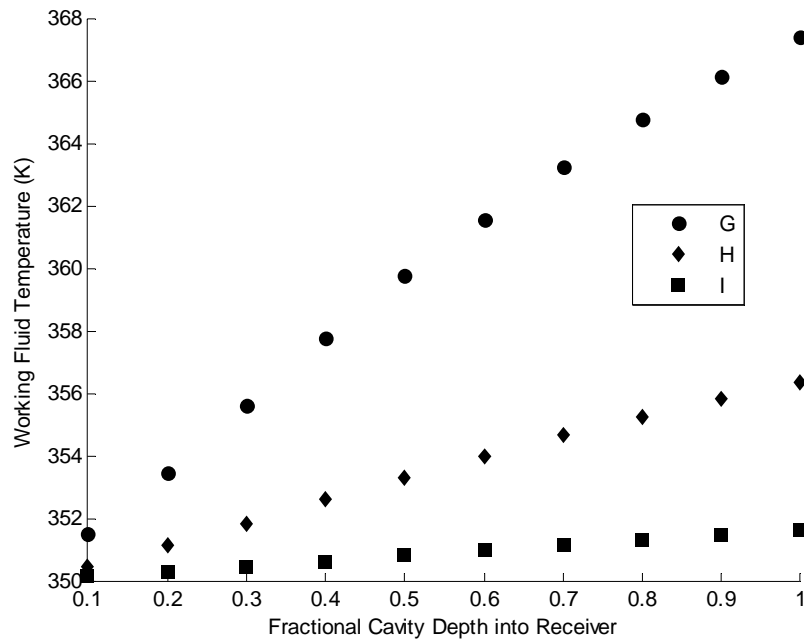
Fig.24. Effect of helical pipe diameter on work fluid temperature (K) through coil segment for case G,H, and I (δ=0.015, 0.025, and 0.050), for inlet velocity of 1 m/s, qsolar of 10 kW, turbulent Reynolds number of 13,000, 22,000, and 43,000 and heat convection coefficients of 5,050, 4,900, and 4,750 W/(m^2*K) respectively.

Further investigation into the net heat transfer rate of the changing diameter of helical pipe, demonstrated for laminar flow, case G, H, and I, 0.021 kg/s per kW, 0.058 kg/s per kW, and 0.23 kg/s per kW for 1 kW respectively and 0.0021 kg/s per kW, 0.0058 kg/s per kW, and 0.023 kg/s per kW for 10 kW respectively, exhibited a distribution with a local maximum, with fractional cavity receiver depth of 0.3-0.5, experiencing the highest net heat transfer rate (Figs. 25-26). And as observed earlier, the onset of turbulent flow, for case G, H ,and I, 0.2081 kg/s per kW, 0.580 kg/s per kW, 2.31 kg/s per kW for 1 kW respectively and 0.02081 kg/s per kW, 0.0580 kg/s per kW, and 0.231 kg/s per kW for 10 kW respectively, results in similar behavior of fluid and thermal characteristics of the flow, as evidenced by behavior of the net heat transfer rates (Figs. 26-27).

Fig.25. Effect of helical pipe diameter on work fluid temperature (K) through coil segment for case G,H, and I (δ=0.015, 0.025, and 0.050), for inlet velocity of 0.1 m/s, qsolar of 1 kW, laminar Reynolds number of 1,300, 2,200, and 4,300 and heat convection coefficients of 850, 733, and 650 W/(m^2*K) respectively.
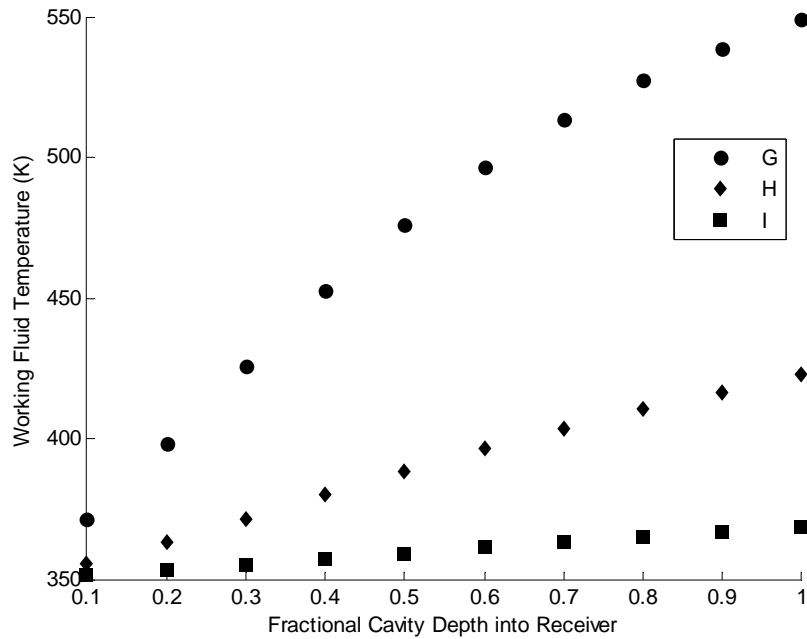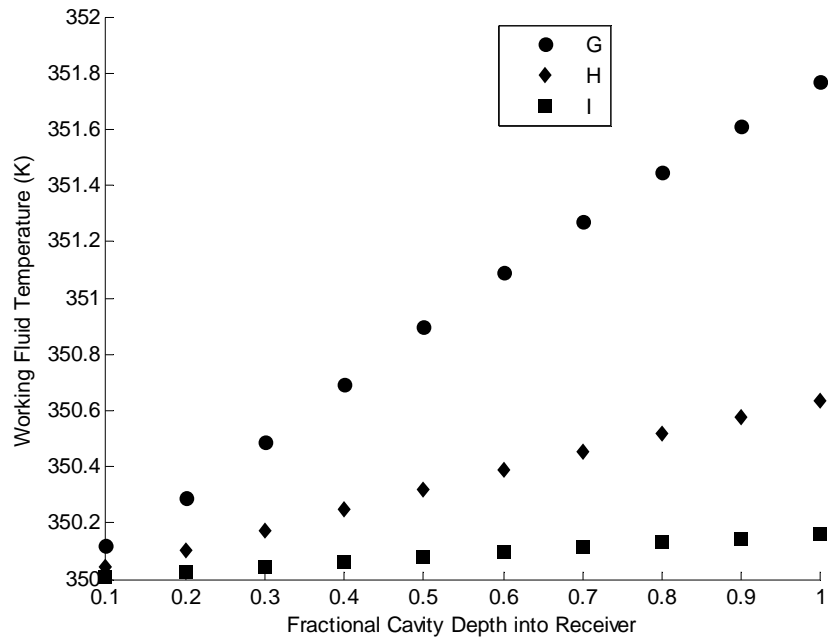
Fig.26. Effect of helical pipe diameter on work fluid temperature (K) through coil segment for case G,H, and I (δ=0.015, 0.025, and 0.050), for inlet velocity of 0.1 m/s, qsolar of 10 kW, laminar Reynolds number of 1,300, 2,200, and 4,300 and heat convection coefficients of 850, 733, and 650 W/(m²*K) respectively.
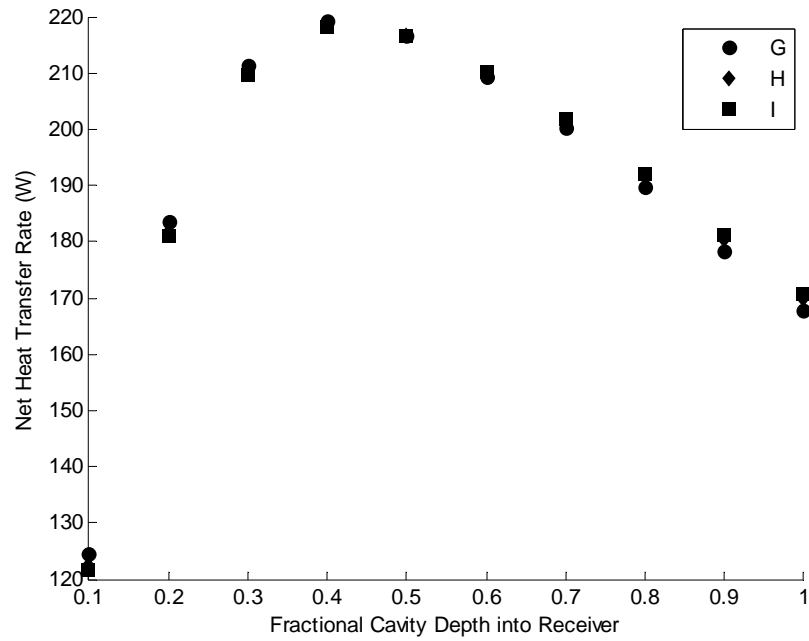
Fig.27. Effect of helical pipe diameter on net heat transfer rate (W) through coil segment for case G,H, and I (δ=0.015, 0.025, and 0.050), for inlet velocity of 1 m/s, qsolar of 1 kW, turbulent Reynolds number of 13,000, 22,000, and 43,000 and heat convection coefficients of 5,050, 4,900, and 4,750 W/(m^2*K) respectively.
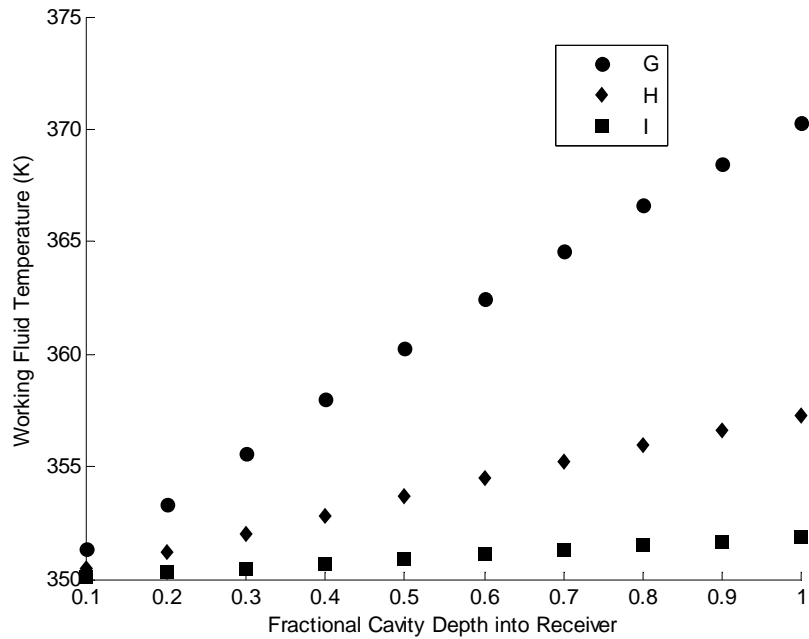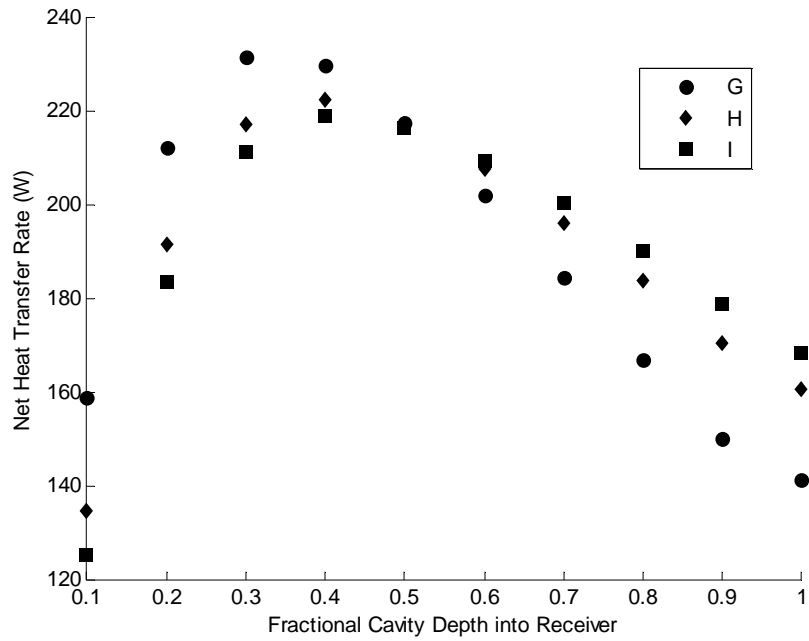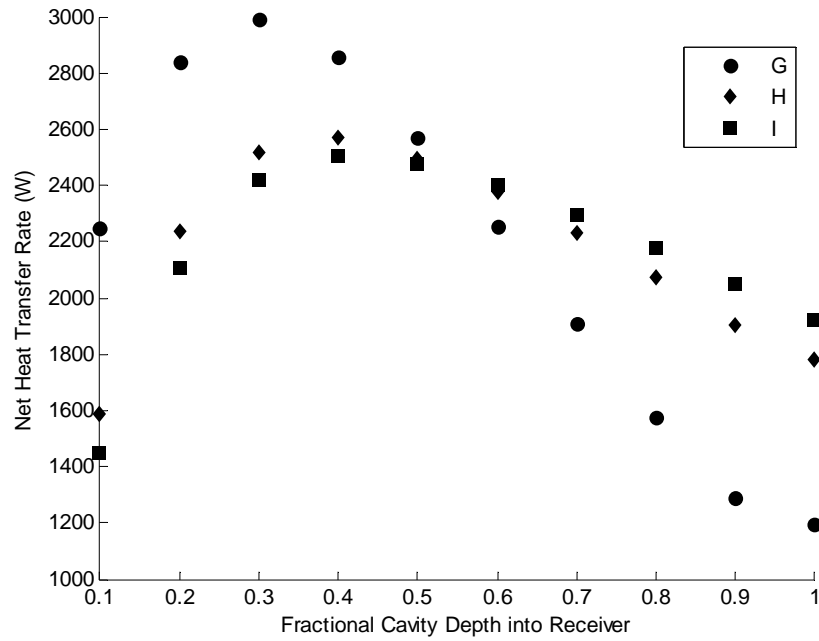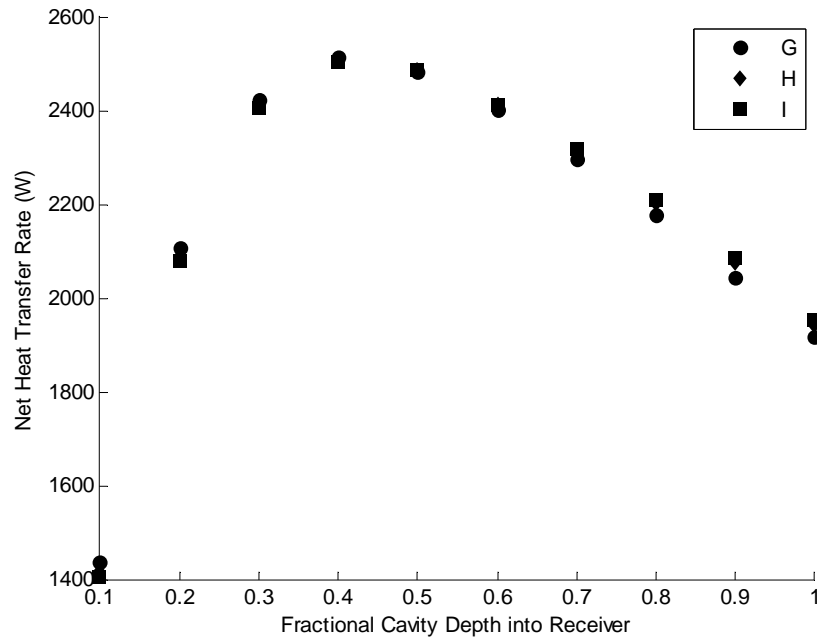
Fig.28. Effect of helical pipe diameter on net heat transfer rate (W) through coil segment for case G,H, and I (δ=0.015, 0.025, and 0.050), for inlet velocity of 1 m/s, qsolar of 10 kW, turbulent Reynolds number of 13,000, 22,000, and 43,000 and heat convection coefficients of 5,050, 4,900, and 4,750 W/(m^2*K) respectively.

It is apparent that changes in the helical pipe diameter, di, will result in shifts in the fluid and thermal characteristics of the pipe flow. Hence increasing the helical pipe diameter, will not only increase the Reynolds number, critical Reynolds number, but also increase the Nusslets number. As turbulent flow is onset, the curvature, δ, is also almost negligible, hence the diameter of the helical pipe, plays the largest role, in determining the heat convection coefficient of the flow. Even as diameter of the helical pipe increases, turbulent flow experiences relatively similar heat convection coefficients of flow, accounting for the behavior of the working fluid temperature and net heat transfer rates of the coil (Figs. 23, 24, 27, and 28).

It is speculated that increasing the helical pipe diameter past 1,000 mm, will result in lower heat convection coefficients of flow, and given an increase in mass flow rate, the outlet temperature of flow will be significantly lower than those for pipes below 100 mm.

Summary of Geometric Effects on Thermal Dynamics and Losses of System

The following investigation details the effects of the cavity receiver length, aperture diameter, and helical pipe diameter on the thermal dynamics of the cavity receiver. In summary, it is demonstrated that tightly packed systems, l=1.1 and h=1.4, demonstrate higher working fluid temperatures for both laminar and turbulent conditions in comparison to medium and loosely packed systems, l=1.5, h=1.9, l=2, and h=2.5 respectively in Figs. 29-30.
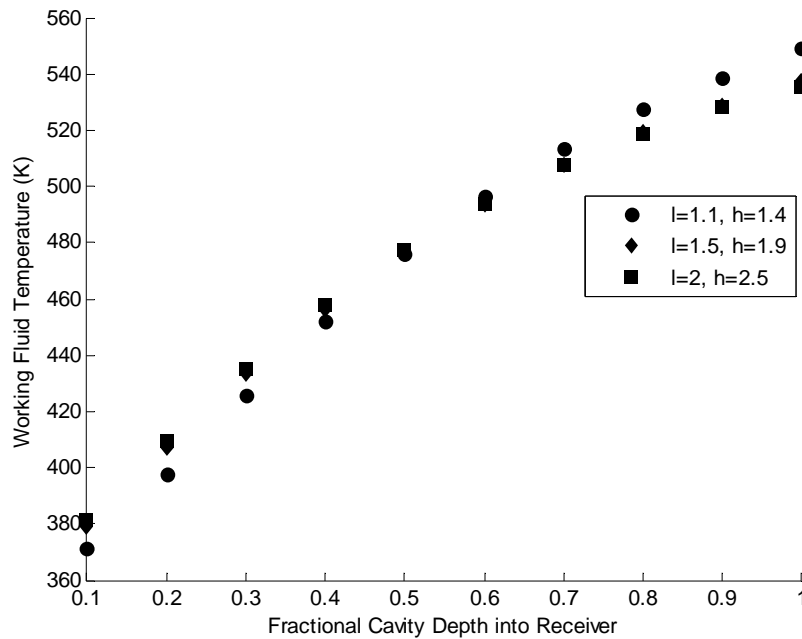
Fig. 29. Effect of coil packing in cavity receiver on working fluid temperature for case A,B, and C (l=1.1, 1.5, and 2) for inlet velocity of 1 m/s, qsolar of 10 kW, laminar Reynolds number of 1,300, and heat convection coefficient of 850 W/(m^2*K).
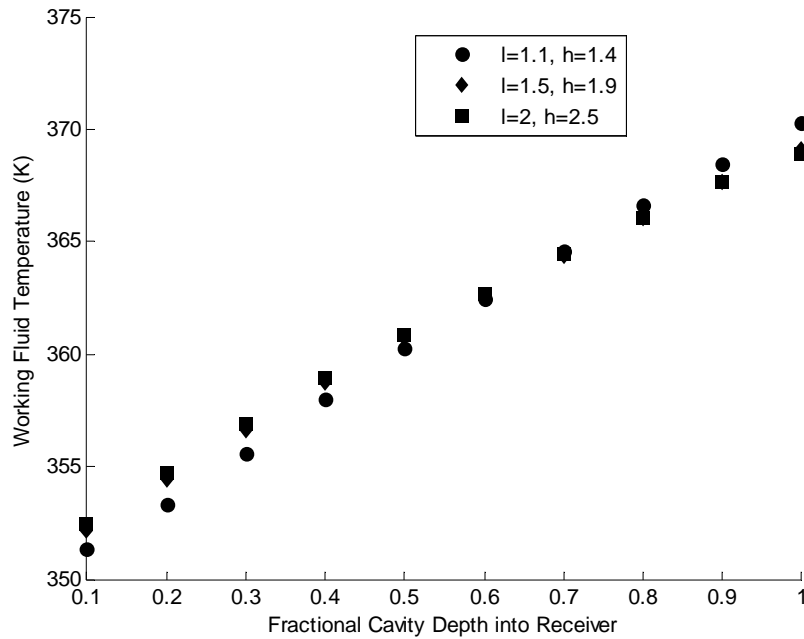
Fig.30. Effect of coil packing in cavity receiver on working fluid temperature for case A,B, and C (l=1.1, 1.5, and 2) for inlet velocity of 1 m/s, qsolar of 10 kW, turbulent Reynolds number of 13,000, and heat convection coefficient of 5,050 W/(m^2*K).

Tightly packed systems, l=1.1 and h=1.4, not only demonstrate higher working fluid temperatures, but also net heat transfer distributions with local maxima, with highest net heat transfer rate in the middle of the cavity receiver, in comparsion to loosely packed systems, l=2 and h=2.5, which have decreasing linear like net heat transfer distribution with increasing fractional cavity receiver depth for both laminar and turbulent flow conditions (Figs. 31-32).
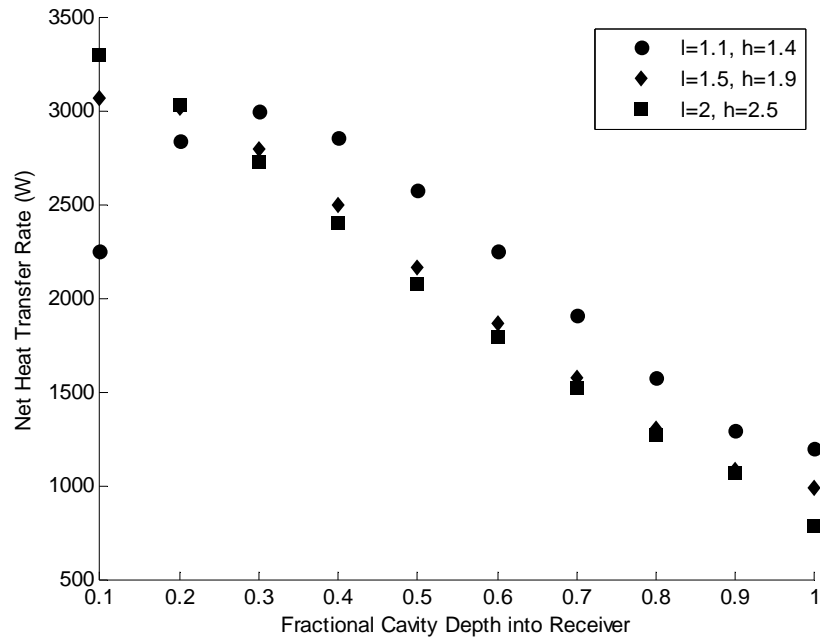
Fig.31. Effect of coil packing in cavity receiver on net heat transfer for case A,B, and C (l=1.1, 1.5, and 2) for inlet velocity of 0.1 m/s, qsolar of 10 kW, laminar Reynolds number of 1,300, and heat convection coefficient of 850 W/(m^2*K).
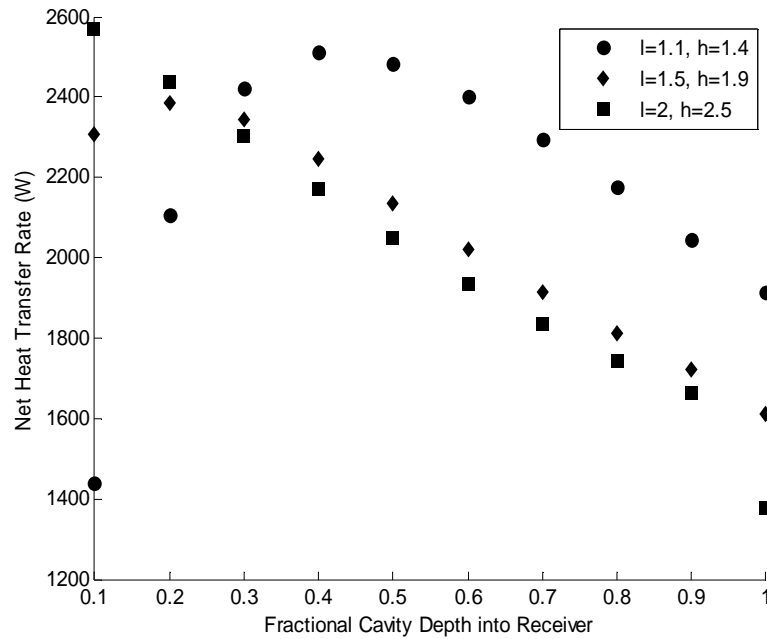
Fig.32. Effect of coil packing in cavity receiver on net heat transfer for case A,B, and C (l=1.1, 1.5, and 2) for inlet velocity of 1 m/s, qsolar of 10 kW, laminar Reynolds number of 13,000, and heat convection coefficient of 5,050 W/(m^2*K).

The investigation of the effect of aperture diameter demonstrated that increasing aperture size, from a=8.0, c=8.0, e=11.0 to a=1.3, c=1.3, and e=1.8, results in lower working fluid temperatures for both laminar and turbulent conditions (Figs. 33-34).
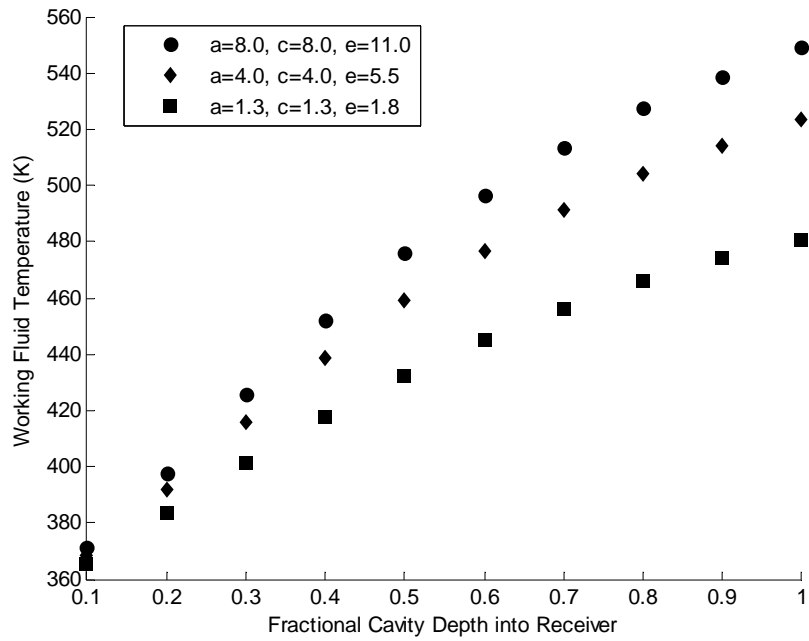
Fig.33. Effect of aperture diameter on working fluid temperature for case D, E, and F (a and c=8,4, and 1.3), for inlet velocity of 0.1 m/s, qsolar of 10 kW, laminar Reynolds number of 1,300, and heat convection coefficient of 850 W/(m^2*K).
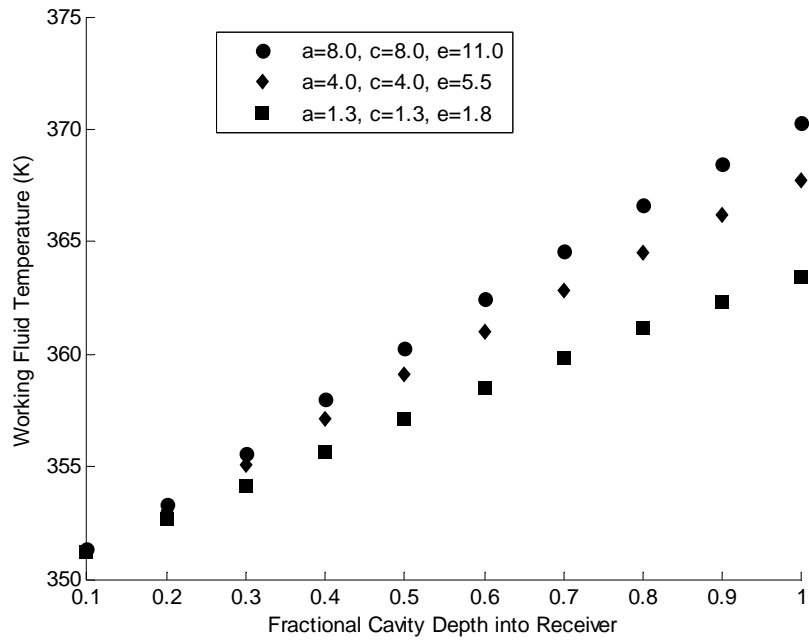
Fig.34. Effect of aperture diameter on working fluid temperature for case D, E, and F (a and c=8,4, and 1.3), for inlet velocity of 1 m/s, qsolar of 10 kW, turbulent Reynolds number of 13,000, and heat convection coefficient of 5,050 W/(m^2*K).

Similarly, increasing the aperture size, from a=8.0, c=8.0, e=11.0 to a=1.3, c=1.3, and e=1.8, resulted in lower net heat transfer distributions, despite similar distribution behavior for varying aperture size for both laminar and turbulent conditions (Figs. 35-36).
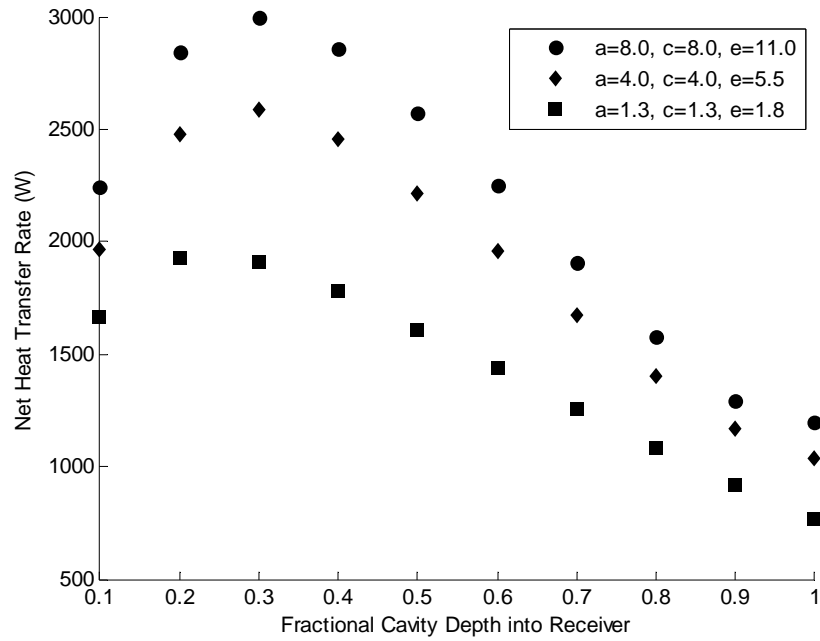
Fig.35. Effect of aperture diameter on net heat transfer rate for case D,E, and F (a and c=8,4, and 1.3), for inlet velocity of 0.1 m/s, qsolar of 10 kW, laminar Reynolds number of 1,300, and heat convection coefficient of 850 W/(m²*K).
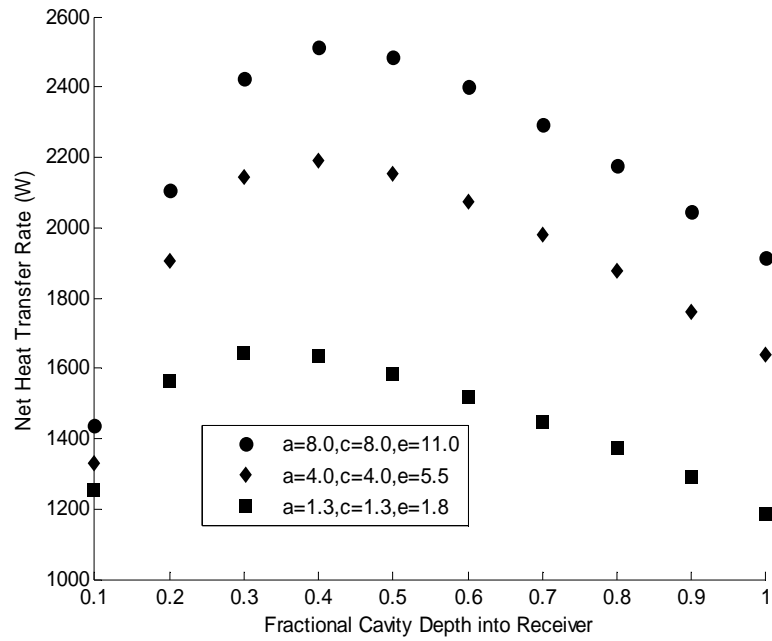
Fig.36. Effect of aperture diameter on net heat transfer rate for case D, E, and F (a and c=8,4, and 1.3), for inlet velocity of 1 m/s, qsolar of 10 kW, turbulent Reynolds number of 13,000, and heat convection coefficient of 5,050 W/(m^2*K).

The investigation lastly concluded that decreasing helical pipe size, from δ=0.050, N=25.0 to δ=0.0015, N=63.0, resulted in higher working fluid temperatures for both laminar and turbulent conditions (Figs. 37-38).
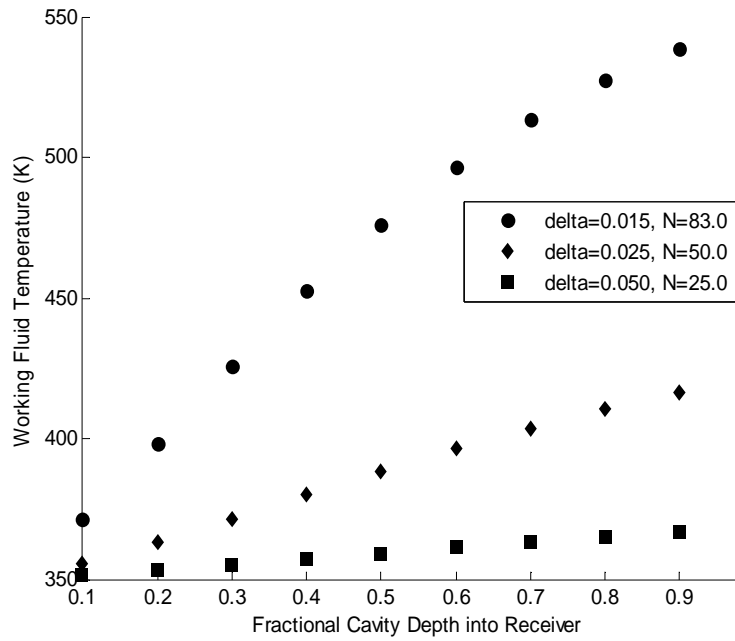
Fig.37. Effect of helical pipe diameter on work fluid temperature (K) through coil segment for case G,H, and I (δ=0.015, 0.025, and 0.050), for inlet velocity of 0.1 m/s, qsolar of 10 kW, laminar Reynolds number of 1,300, 2,200, and 4,300 and heat convection coefficients of 850, 733, and 650 W/(m^2*K) respectively.
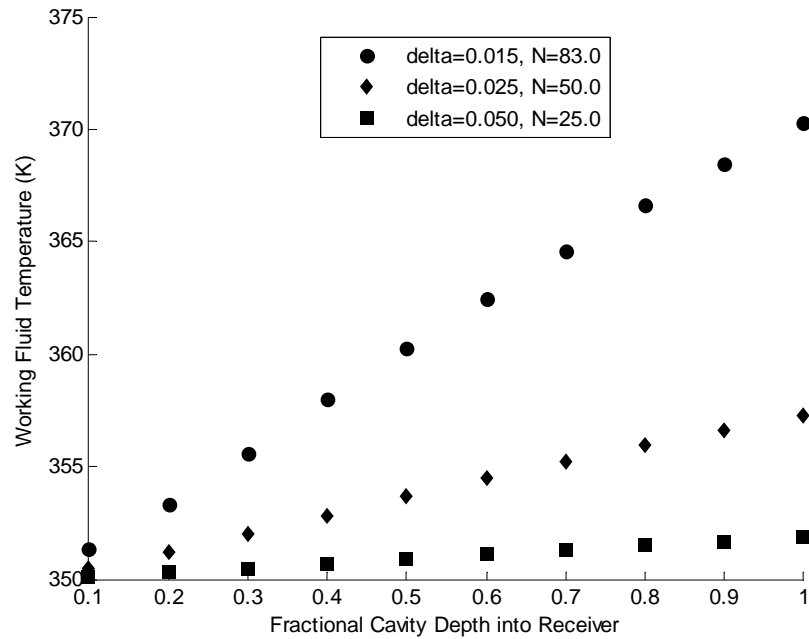
Fig.38. Effect of helical pipe diameter on work fluid temperature (K) through coil segment for case G,H, and I (δ=0.015, 0.025, and 0.050), for inlet velocity of 0.1 m/s, qsolar of 10 kW, laminar Reynolds number of 1,300, 2,200, and 4,300 and heat convection coefficients of 850, 733, and 650 W/(m^2*K) respectively.

Lastly for given laminar and turbulent flow conditions, smaller helical pipe diameters, δ=0.0015, N=63.0, result in higher net heat transfer distributions, with the highest heat transfer at the middle of the cavity receiver, in comparison to larger helical pipe diameters, δ=0.050, N=25.0 (Figs. 39-40).
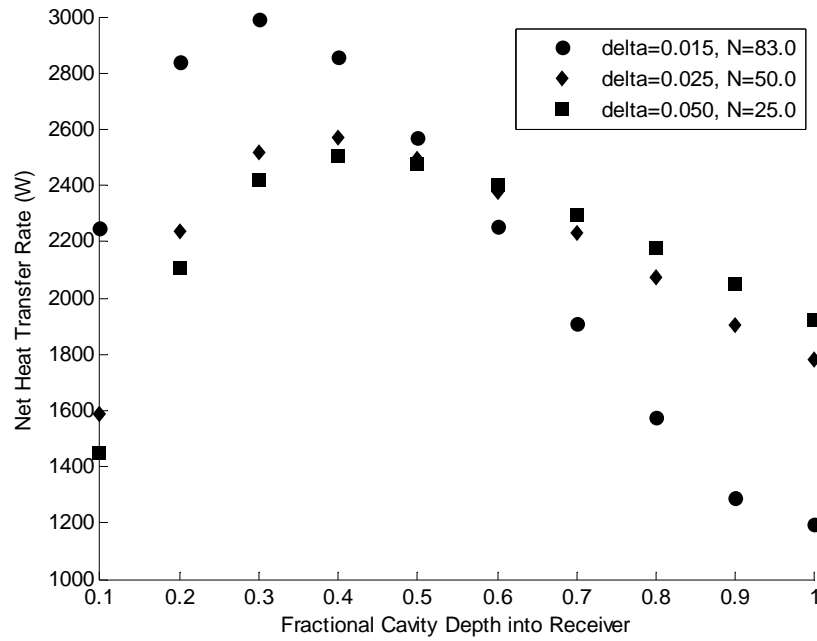
Fig.39. Effect of helical pipe diameter on work fluid temperature (K) through coil segment for case G,H, and I (δ=0.015, 0.025, and 0.050), for inlet velocity of 1 m/s, qsolar of 10 kW, turbulent Reynolds number of 13,000, 22,000, and 43,000 and heat convection coefficients of 5,050, 4,900, and 4,750 W/(m^2*K) respectively.
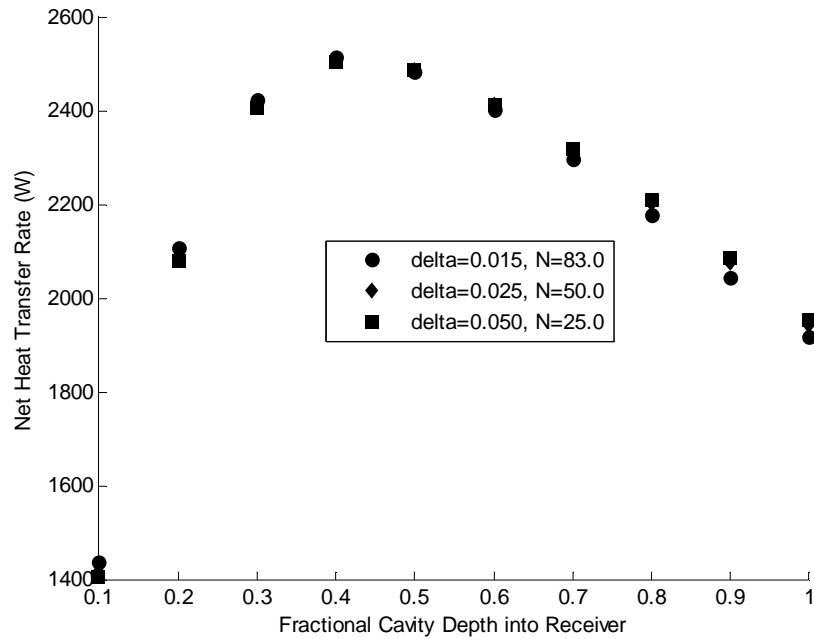
Fig.40. Effect of helical pipe diameter on net heat transfer rate (W) through coil segment for case G,H, and I (δ=0.015, 0.025, and 0.050), for inlet velocity of 1 m/s, qsolar of 10 kW, turbulent Reynolds number of 13,000, 22,000, and 43,000 and heat convection coefficients of 5,050, 4,900, and 4,750 W/(m^2*K) respectively.

From these three separate investigations, it is concluded that an optimal design of a cavity receiver would be one that would be tightly packed, minimized in aperture and helical pipe diameter.

Towards the Design of an Optimal Solar Cavity Receiver System

The following results and analysis, demonstrate not only the validity of the theoretical model and the simulation tool in respect to modeling the radiative and convective heat transfer in the system, but also give insight into possible design specifications for a solar cavity receiver.

The current modeling of the cavity receiver has been done for steady operating conditions for a few parametric variations. Since it does not take into account transient behavior, further work is needed before these results can be applicable for a solar thermal cavity receiver design. As mentioned earlier, this model accounts for the conservation of continuity and energy, neglecting friction, temperature dependent property changes,

55

pressure drops, and other atmospheric interactions e.g. heating of the atmospheric gas inside the cavity receiver. These results, rather through a number of different geometric conformations and fluid-thermal characteristics, suggest design and test conditions of possible interest, through comparisons of several dimensionless variables, for the solar cavity receiver.

The results suggest the following design and test conditions of interest (Table 9), in relation to higher working fluid temperatures and net heat transfer rates of the coil.

Table 9. Suggested design and test conditions for solar cavity receiver system

Case	l	h	a	b	c	e	δ	N
A/D/G	1.1	1.4	8.0	1.0	8.0	11.0	0.015	83.0

For insight into realistic optimal design for a solar cavity receiver, two additional popular heat transfer fluids were utilized (Table 10), Therminol VP-1 [28] and Dynalene EG [29].

Table 10. Working heat transfer fluid properties for Solar Salt, 60% $NaNO_3$, 40% KNO_3, Therminol VP-1, and 70 % Dynalene EG

Heat Transfer Fluid	Liquid Phase Stable Temperature Upper Limit Value (K)	Specific Heat @ 100 C (J/(kg*K))	Density @ 100 C (kg/ m^3)	Viscosity @ 100 C (Pa*s)	Thermal Conductivity @ 100 C (W/(m*K))
Solar Salt	803	1,600	1,970	0.07	0.14
Therminol VP-1	673	1,775	999	0.10	0.13
Dynalene EG	394	3,243	1,052	0.0083	0.35

These fluids were simulated at the suggested optimal design conditions (Table 9), for 1, 5, and 15 kW solar inputs at laminar flow rates and heat convection coefficients as given in Table 11.

Table 11. Heat transfer fluid conditions for design of an optimal solar cavity receiver

Heat Transfer Fluid	Solar Input (kW)	Velocity (m/s)	$\dot{m}$ (kg/s)	Re_D	Nu_D	hfi (W/(m²*K))
Solar Salt	15	0.10	0.022	34	11	123
	15	0.30	0.067	101	17	203
Therminol VP-1	5	0.10	0.011	12	8	86
	5	0.30	0.034	36	12	133
Dynalene EG	1	0.10	0.012	152	12	344
	1	0.30	0.036	456	20	581

The results demonstrated show upper temperatures of 750, 540, and 360 K are achieved for a laminar flow rate of 0.1 m/s, corresponding to Reynolds numbers of 34, 12, 152 and 0.0015 kg/s per kW, 0.022 kg/s per kW, and 0.012 kg/s per kW for the Solar Salt, Therminol VP-1, and Dynalene EG fluids respectively (Fig. 41).
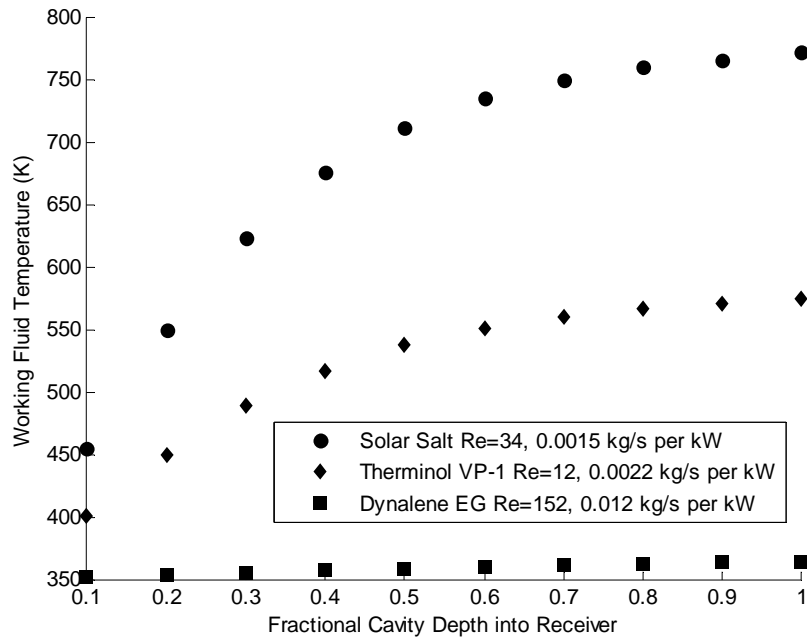
Fig.41. Working fluid temperature (K) of Solar Salt, Re_D=34, 0.0015 kg/s per kW, Therminol VP-1, Re_D=12, 0.0022 kg/s per kW, and Dynalene EG, Re_D=152, 0.012 kg/s per kW for laminar flow and heat transfer conditions.

It is interesting to note that at the solar input 15 kW, the solar salt nearly achieved its critical stable temperature limit of 803 K (Table 10) as does the 70% Dynalene EG at 5 kW with a working temperature of 364 K (Fig. 41). It is estimated based on the optimal conditions (Table 9), a solar input of 5-10 kW at laminar flow rates prescribed (Table 11), would be appropriate for the Therminol VP-1 to still remain stable in its liquid phase (Fig. 41).

As flow increased from 0.1 to 0.3 m/s, it is interesting to observe that the working fluid temperatures of the fluid decreased significantly. With the onset of higher flow velocity, the Solar Salt exhibited low temperatures throughout the coil, temperatures that represent its solid phase, rather than its liquid phase (Fig. 42).
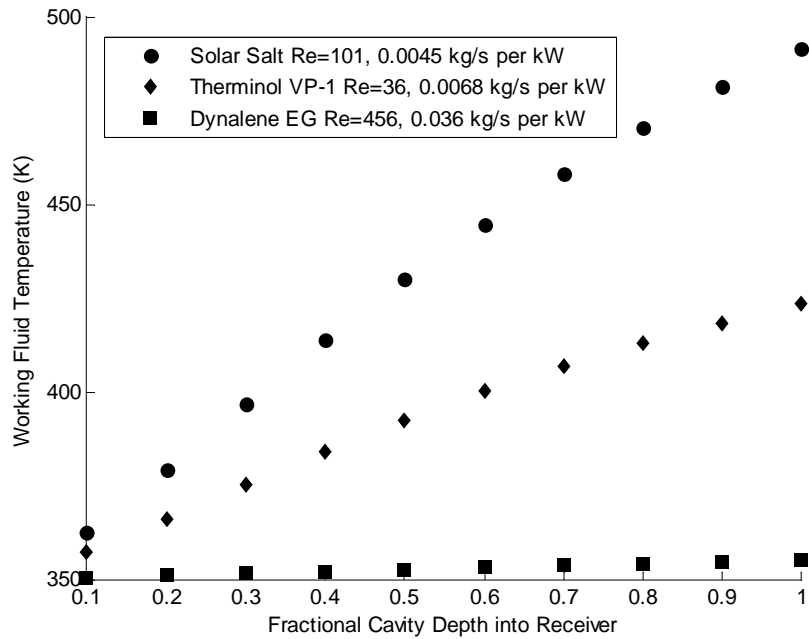
Fig.42. Working fluid temperature (K) of Solar Salt, $Re_D=101$, 0.0045 kg/s per kW, Therminol VP-1, $Re_D=36$, 0.0068 kg/s per kW, and Dynalene EG, $Re_D=456$, 0.036 kg/s per kW for laminar flow and heat transfer conditions.

Further investigation of the net transfer behavior, demonstrated for laminar flow velocity of 0.1 m/s corresponding to Reynolds number of 34, 0.0015 kg/s per kW for Solar Salt, Reynolds number of 12, 0.0022 kg/s per kW for Therminol VP-1, and Reynolds number of 152, 0.012 kg/s per kW for Dynalene EG, the highest net heat transfer occurred at top of the cavity receiver, with net heat transfer rate decreasing with fractional cavity receiver depth (Fig. 43).
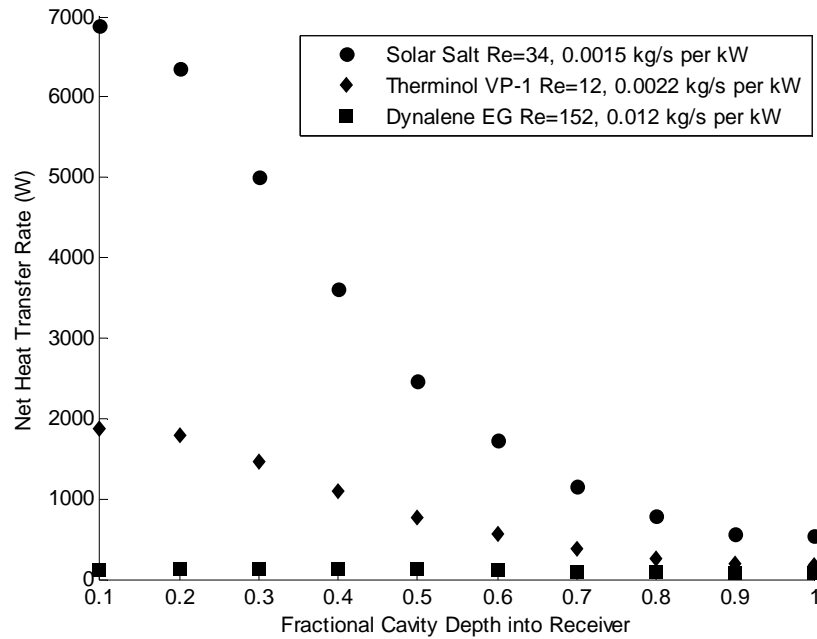
Fig.43. Net heat transfer rate of Solar Salt, Re_D=34, 0.0015 kg/s per kW, Therminol VP-1, Re_D=12, 0.0022 kg/s per kW, and Dynalene EG, Re_D=152, 0.012 kg/s per kW for laminar flow and heat transfer conditions.

As flow velocity is increased to 0.3 m/s, Reynolds number of 101, 0.0045 kg/s per kW for Solar Salt, Reynolds number of 36, 0.0068 kg/s per kW for Therminol VP-1, Reynolds number of 456, 0.036 kg/s per kW for Dynalene EG, the net heat transfer rate exhibited a distribution with a local maximum at 0.1, the middle of the cavity receiver having the largest net heat transfer rate (Fig. 44).
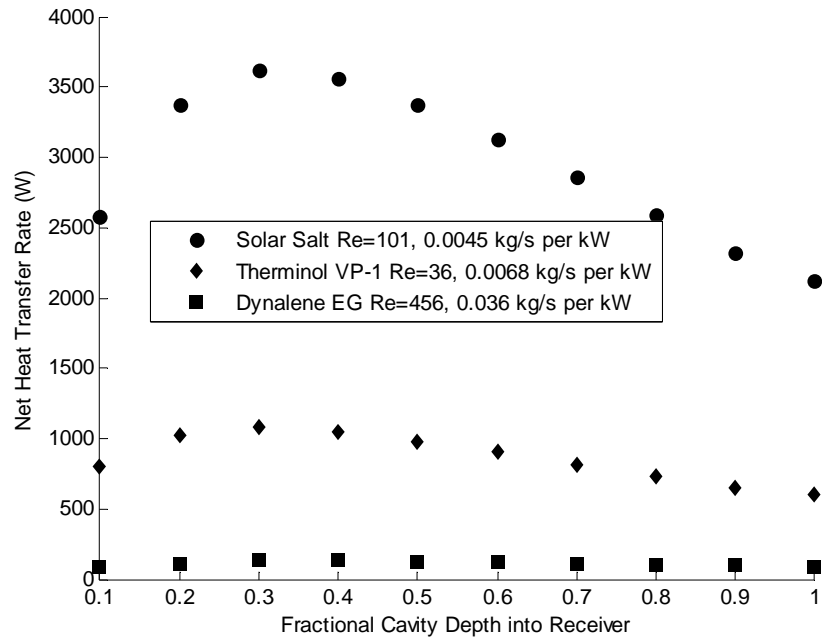
Fig.44. Net heat transfer rate of Solar Salt, Re=101, 0.0045 kg/s per kW, Therminol VP-1, Re=36, 0.0068 kg/s per kW, and Dynalene EG, Re=456, 0.036 kg/s per kW for laminar flow and heat transfer conditions.

It is interesting to note based on these results, at low flow velocities, as 0.1 m/s, convection within the helical coil is as not as a significant factor as the radiation exchange between the aperture and the coils. Hence geometry plays the most important part in determining the net heat transfer rate and working fluid temperatures (Figs. 41, 43). As flow velocities increase to 0.3 m/s, convection starts to play a part in the thermal dynamics of the system, and hence thermal behavior of the flow is determined by radiation exchange and convection loss (Figs. 42, 44).

Table 12. Energy generated and efficiency of Solar Salt, Therminol VP-1, and Dynalene EG for prescribed laminar conditions.

Heat Transfer Fluid	Velocity (m/s)	Re_D per kW	$E_{gen}(W)$	$\in$ (%)
Solar Salt	0.1	2.3	14,800	99
	0.3	6.7	15,000	100
Therminol VP-1	0.1	2.4	4374	87
	0.3	7.2	4406	88
70 % Dynalene EG	0.1	152	546	55
	0.3	456	466	47

As demonstrated earlier in analyzing the effective size of the aperture for the cavity receiver in respect to thermal dynamics and losses, as the solar input increases, the efficiency tends to increase as well, given a fluid, as evidenced by the lower efficiency levels of Dynalene EG, 47% and 55 % at 1 kW of solar input in comparison to the higher efficiency levels of Solar Salt, 99% and 100 % at 15 kW of solar input (Table 12).

Given optimum design of the solar cavity receiver, with healthy solar inputs of 5 to 25 kW with reasonable laminar flow rates, higher working fluid temperatures and net heat transfer rates in the coil system can achieved. It is expected that as flow velocity increases, past 1 m/s, lower working fluid temperatures will be achieved, as convection starts to dominate over radiation exchange, especially when solar input is low, as on a cloudy day. Higher flow velocities may mean larger operating costs and imply a need for higher end point concentrators for large solar inputs into the cavity receiver system.

Chapter 5. Conclusions and Suggestions for Future Research

A numerical analysis of a solar cavity receiver is performed to bring out the characteristics leading to an optimal design. This investigation characterizes the thermal performance a of a solar cavity receiver as functions of geometrical parameters such as cavity receiver length, aperture diameter, and helical pipe diameter.

The effect of the cavity receiver length on receiver performance is described by the following:

- Tightly packed cavity receivers, l=1.1 and h=1.4, where l is the ratio of cavity length to coil length and h is ratio of cavity length to diameter of the receiver, demonstrate higher working fluid temperatures for both laminar and turbulent conditions in comparison to medium and loosely packed cavity receivers, l=1.5, h=1.9 and l=2, h=2.5.

- Tightly packed systems, l=1.1 and h=1.4, demonstrate net heat transfer distributions with local maxima, with highest net transfer in the middle of the cavity receiver, in comparsion to loosely packed systems, 1=2 and h=2.5, which have decreasing linear like net heat transfer distributions with increasing fractional cavity receiver depth for both laminar and turbluent flow conditions.

Tightly packed cavity receivers, l=1.1 and h=1.4, were shown to have the highest working fluid temperatures and net heat transfer distributions.

The investigation of the effect of the aperture size on cavity receiver demonstrated:

- Increasing aperture size, from a=8.0, c=8.0, e=11.0 to a=1.3, c=1.3, and e=1.8, where a is ratio of length of cavity receiver to diameter of cavity receiver, c is ratio of diameter of helical coil to diameter of aperture, and e is ratio of length of cavity receiver to diameter of aperture results in lower working fluid temperatures for both laminar and turbulent conditions.

- Increasing the aperture size, from a=8.0, c=8.0, e=11.0 to a=1.3, c=1.3, and e=1.8, resulted in lower net heat transfer distributions, despite similar heat

transfer behavior for varying aperture size for both laminar and turbulent conditions.

Further the investigation demonstrated that minimization of aperture size, a=8.0, c=8.0, e=11.0, not only minimizes of convective losses, but also increases thermal efficiency, given appropriate solar input.

The investigation of the effect of the helical pipe diameter on cavity receiver demonstrated that:

- Decreasing helical pipe size, from δ=0.050, N=25.0 to δ=0.0015, N=63.0, where δ is the ratio of diameter of helical coil to diameter of coil pipe and N is ratio of length of helical coil to diameter of helical pipe, resulted in higher working fluid temperatures for both laminar and turbulent conditions.
- Given laminar and turbulent flow conditions, smaller helical pipe diameters, δ=0.0015, N=63.0, result in higher net heat transfer distributions, with the highest heat transfer at the middle of the cavity receiver, in comparison to larger helical pipe diameters, δ=0.050, N=25.0.

The investigation further demonstrated that minimization of helical pipe size, δ=0.0015, N=63, was shown to have the highest working fluid temperatures and net heat transfer distributions.

Based on these observations and conclusions, an investigation of the optimal cavity receiver design was conducted. A cavity receiver design with dimensionless geometric parameters of l=1.1, h=1.4, a=8.0, c=8.0, e=11.0, δ=0.0015, and N=63 was chosen for the investigation of the effect of three different heat transfer fluids, Solar Salt, Therminol VP-1, and Dynalene EG.

Based on this investigation it was concluded that:

- For qsolar of 15, 5, and 1 kW, larger temperatures of 750, 540, and 360 K are achieved for a laminar flow rate of 0.1 m/s, corresponding to Reynolds numbers of 34, 12, 152 and 0.0015 kg/s per kW, 0.022 kg/s per kW, and 0.012 kg/s per kW for the Solar Salt, Therminol VP-1, and Dynalene EG fluids respectively.

64

- As flow increased from 0.1 to 0.3 m/s, the working fluid temperatures of the fluid decreased significantly. With the onset of higher flow velocity, the Solar Salt exhibited low temperatures throughout the coil, temperatures that represent its solid phase, rather than its liquid phase.

- For laminar flow velocity of 0.1 m/s corresponding to Reynolds number of 34, 0.0015 kg/s per kW for Solar Salt, Reynolds number of 12, 0.0022 kg/s per kW for Therminol VP-1, and Reynolds number of 152, 0.012 kg/s per kW for Dynalene EG, the highest net heat transfer occurred at the top of the cavity receiver, with net heat transfer rate decreasing with increasing fractional cavity receiver depth.

- As flow velocity increased to 0.3 m/s, corresponding to Reynolds number of 101, 0.0045 kg/s per kW for Solar Salt, Reynolds number of 36, 0.0068 kg/s per kW for Therminol VP-1, Reynolds number of 456, 0.036 kg/s per kW for Dynalene EG, the net heat transfer rate exhibited a distribution with a local maxima, the middle of the cavity receiver having the largest net heat transfer rate.

- As the solar input increases, the efficiency tends to increase as well, given a fluid, as evidenced by the lower efficiency levels of Dynalene EG, 47% and 55 % at 1 kW of solar input in comparison to the higher efficiency levels of Solar Salt, 99% and 100 % at 15 kW of solar input.

It can be additionally concluded that:

- The cavity receiver with dimensionless geometric parameters of l=1.1, h=1.4, a=8.0, c=8.0, e=11.0, and δ=0.0015, **presents an optimal design** that can achieve high working fluid temperatures and net heat transfer rates, given solar inputs of 5 to 25 kW and reasonable laminar flow rates.

At the present, the results presented are preliminary, as given by the steady state nature of the analysis conducted here that used conservation of energy as the primary basis in this investigation. These results cannot be directly correlated at this time to any current research in the solar cavity receiver field that may have transients in power input.

It is evident from this preliminary step towards an optimal cavity receiver design that additional components to the simulation tool must be implemented as related to:

- Frictional effects for flow in pipes
- Temperature dependent property changes for the fluid
- Pressure drops for flow
- Heating of the atmospheric air in the cavity receiver

More importantly, experimental results for the designated test conditions in this investigation must be obtained, to verify the current results and to further improve the analytical basis used in this study.

It is only with and after such experimental results, any real, efficient cavity can receivers be constructed and implemented. This simulation tool can be converted from steady to transient state model for simulation, testing, and development purposes of actual solar thermal cavity receivers. A dynamic, robust transient model of the thermal dynamics of the solar cavity receiver system would serve as strong simulation tool for the entire solar cavity receiver community.

References

1. Principles of Solar Engineering. Y. Goswami and F. Kreith. **CRC Press**: 2000.
2. High temperature molten salt thermal energy storage systems for solar applications. R. Petri and T. Claar. **NASA Lewis Research Center**: 1980, 184-190.
3. Central receiver system solar power plant using molten salt as heat transfer fluid. J. Ortega, J. Burgaleta, F. Tellez. **Journal of Solar Energy Engineering**: 2008, 1-6.
4. Study on design of molten salt solar receivers for beam-down solar concentrator. H. Hasuike, Y. Yoshizawa, A. Suzuki. **Solar Energy**: 2006, 1255-1262.
5. Investigations on heat losses from a solar cavity receiver. M. Prakash, S. Kedare, and J. Nayak. **Solar Energy**: 2009, 157-170.
6. Numerical investigations of natural convection heat loss in modified cavity receiver for fuzzy local solar dish concentrator system. S. Reddy and S. Kumar. **Solar Energy**: 2007, 846-855.
7. An improved model for natural convection heat loss from modified cavity receiver of solar dish concentrator. S. Reddy and S. Kumar. **Solar Energy**: 2009, 1884-1892.
8. Thermal performance simulation of a solar cavity receiver under windy conditions. J. Fang, J. Wei, X. Dong, and Y. Wang. **Solar Energy**: 2011, 126-138.
9. Radiation performance of dish solar concentrator/cavity receiver systems. Y. Shuai, X. Xia, H. Tan. **Solar Energy**: 2008, 13-21.
10. Flow in curved pipes. S. Berger and L. Talbot. **Annual Review Fluid Mechanics**: 1983, 461-512.
11. Heat transfer and pressure loss in helically coiled tubes with turbulent flow. G. Rogers and Y. Mayhew. **International Journal of Heat and Mass Transfer:** 1964, 1207-1216.
12. Entrance region heat transfer in a uniform wall-temperature helical coil with transition from turbulent to laminar flow. C. Kalb, J. Seader. **International Journal of Heat and Mass Transfer**: 1983, 23-32.
13. Heat transfer for laminar flow in curved pipes with uniform wall heat flux. M. Balejova and J. Cakrt. **Acta Technica Csav:** 1977, 183-194.
14. Entrance region heat transfer in uniform wall-temperature helical coil with transition from turbulent to laminar flow. **International Journal of Heat and Mass Transfer**: 1983, 23-32.
15. Fully developed laminar convection from a helical coil. I. Manlapaz and S. Churchill. **Chemical Engineering Communications**: 1981, 185-200.
16. Pressure drop and heat transfer in coils. P. Srinivasan. **Chemical Engineering**: 1968, 11-13.

17. Optimal Reynolds number of laminar forced convection in a helical tube subjected to uniform wall temperature. H. Shokouhmand and M. Salimpour. **International Communications in Heat and Mass Transfer**: 2004, 753-761.
18. Developing turbulent convective heat transfer in helical pipe. C. Lin and M. Ebadian. **International Journal of Heat and Mass Transfer**: 1997, 3861-3873.
19. Pressure drop correlations for flow through regular helical coil tubes. S. Ali. **Fluid Dynamics Research**: 2001, 295-301.
20. An experimental study of pressure drop in helical pipes. S. Liu, A. Afacan, H. Din, J. Masliyah. **Proceedings of the Royal Society**: 1994, 307-316.
21. Stabilization effects in flow through helically coiled pipes. K. Sreenivasan and P. Strykowski. **Experiments in Fluids:** 1983, 31-36.
22. Free convection heat transfer from the outer surface of vertically orientated helical coils in glycerol-water solution. M. Ali. **Heat and Mass Transfer**: 2004, 615-620.
23. An experimental investigation of the frictional pressure drop of steam-water two-phase flow in helical coils. L. Guo, Z. Feng, and X. Chen. **International Journal of Heat and Mass Transfer**: 2001, 2601-2610.
24. Laminar forced convection in the entrance region of helical pipes. C. Lin, P. Zhang, and M. Ebadian. **International Journal of Heat and Mass Transfer**: 1997, 3293-3304.
25. Fundamentals of Heat and Mass Transfer. D. Dewitt and F. Incorporea. **Wiley Higher Education**: 2006.
26. Engineering database liquid Salt thermophysical and thermochemical properties. M. Sohal, M. Ebner, P. Sabharwall, P. Sharpe. **Idaho National Laboratory, US Department of Energy**: 2010, pg. 1-70.
27. Thermal Radiation Heat Transfer. J. Howell and R. Siegel. **CRC Press**: 2010.
28. Therminol VP-1 Heat Transfer Fluids. **Solutia**: **Applied Chemistry and Creative Solutions**: 2012.
29. Dynalene Inhibited Ethylene Glycol Heat Transfer Fluid. **Dynalene Heat Transfer Fluids**: 2012.

Appendices

Appendix A: View Factor Relationships

A.1. Aperture to Reflector Surface

In order to characterize the heat exchange between the aperture and the reflector solid circular surface, the view factor relationship [28], "Disk to parallel coaxial disk of unequal radius", (Fig. 45) was used (23).
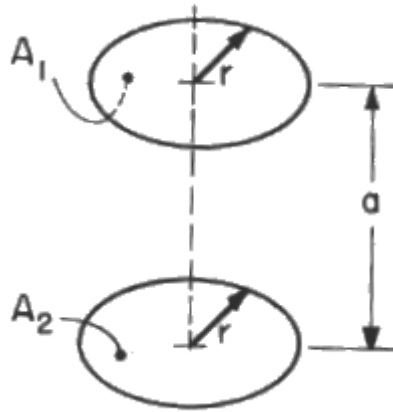
Fig.45. Aperture to reflector view [27]

The governing equation is given by, equation 23

$$F_{1-2} = \frac{1}{2} \left\{ X - \left[X^2 - 4\left(\frac{R_2}{R_1}\right)^2 \right]^{1/2} \right\}$$

(23)

with

$$R_i = \frac{r_i}{a}$$

$$X = 1 + \frac{1 + R_2{}^2}{R_1^2}$$

A.2. Aperture/Reflector/Lid Surface to Helical Coils

In order to characterize the heat exchange between the aperture, the reflector, or lid surface to the inner portion of the helical coils, the view factor relationship [28], "Ring element on base of right circular cylinder to finite circumferential ring on interior of cylinder ", (Fig. 46) was used (24).
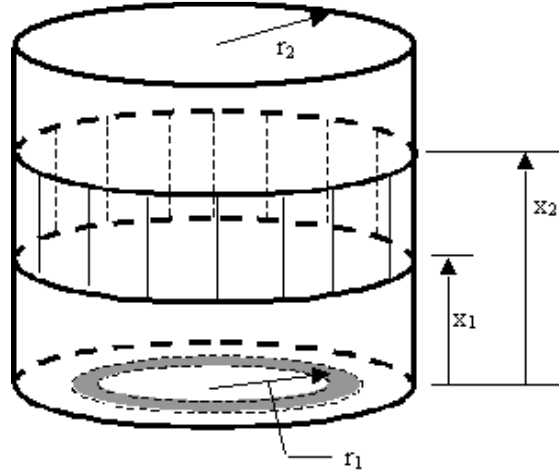
Fig.46. Aperture/reflector/lid to inner coil view [27]

The view factor relationship is given by equation 24.

$$F_{d1-2} = \frac{1}{2}\left[\frac{\left(X_2^2 + R^2 - 1\right)}{\sqrt{\left(X_2^2 + R^2 + 1\right)^2 - 4R^2}} - \frac{\left(X_1^2 + R^2 - 1\right)}{\sqrt{\left(X_2^2 + R^2 + 1\right)^2 - 4R^2}} \right] \tag{24}$$

with

$$X1 = \frac{x1}{r2}$$

$$X2 = \frac{x2}{r2}$$

$$R = \frac{r1}{r2}$$

A.3. Helical Coil to Neighboring Helical Coil

In order to characterize the heat exchange between sections of inner helical coils, the view factor relationship [28], "Identical, parallel, directly opposed rectangles", (Figs. 47-48) was used (25).
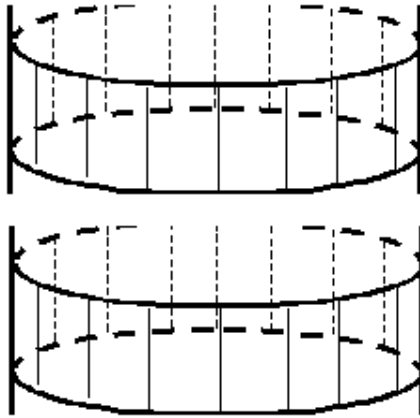
Fig.47. Inner helical coil to neighboring coil view [27]
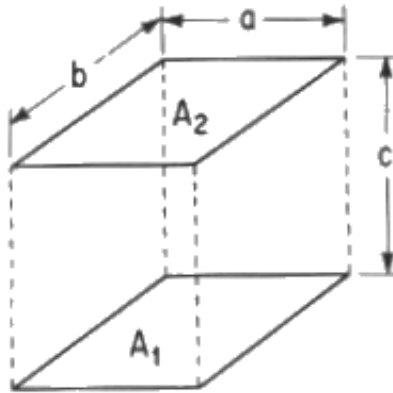
Fig. 48. Inner helical coil to inner helical coil view [27]

$$F_{1-2} = \frac{2}{\pi XY} \left\{ \begin{array}{l} \ln\left[\frac{\left(1+X^2\right)\left(1+Y^2\right)}{1+X^2+Y^2}\right]^{1/2} + X\sqrt{1+Y^2}\,\tan^{-1}\frac{X}{\sqrt{1+Y^2}} \\[3mm] + Y\sqrt{1+X^2}\,\tan^{-1}\frac{Y}{\sqrt{1+X^2}} - X\tan^{-1}X - Y\tan^{-1}Y \end{array} \right\} \qquad (25)$$

with

$$X = \frac{a}{c}$$

$$Y = \frac{b}{c}$$

Appendix B: Simulation Test Cases

In order to develop a simulation tool, test cases were developed as described in Table 13 with prescribed heat transfer fluid.

Table 13. Solar flux, velocity, mass flow, Reynolds, Prandtl, Nusslet , and heat convection coefficient constants for geometric cases A-I

| Case	qsolar (kW)	Velocity (m/s)	$\dot{m}$ (kg/s)	Re_D	Pr	Nu_D	hfi (W/(m^2*K))
A1	1	0.1	0.021	1.3e+003	8.2	18.5	849.8
B1		0.1	0.021	1.3e+003	8.2	18.5	849.8
C1		0.1	0.021	1.3e+003	8.2	18.5	849.8
D1		0.1	0.021	1.3e+003	8.2	18.5	849.8
E1		0.1	0.021	1.3e+003	8.2	18.5	849.8
F1		0.1	0.021	1.3e+003	8.2	18.5	849.8
G1		0.1	0.021	1.3e+003	8.2	18.5	849.8
H1		0.1	0.058	2.2e+003	8.2	26.6	732.60
I1		0.1	0.23	4.33e+003	8.2	47.3	649.70
A2	5	0.1	0.021	1.3e+003	8.2	18.5	849.8
B2		0.1	0.021	1.3e+003	8.2	18.5	849.8
C2		0.1	0.021	1.3e+003	8.2	18.5	849.8
D2		0.1	0.021	1.3e+003	8.2	18.5	849.8
E2		0.1	0.021	1.3e+003	8.2	18.5	849.8
F2		0.1	0.021	1.3e+003	8.2	18.5	849.8
G2		0.1	0.021	1.3e+003	8.2	18.5	849.8
H2		0.1	0.058	2.2e+003	8.2	26.6	732.6
I2		0.1	0.23	4.33e+003	8.2	47.3	649.70
A3	10	0.1	0.021	1.3e+003	8.22	18.5	849.8
B3		0.1	0.021	1.3e+003	8.22	18.5	849.8
C3		0.1	0.021	1.3e+003	8.22	18.5	849.8
D3		0.1	0.021	1.3e+003	8.22	18.5	849.8
E3		0.1	0.021	1.3e+003	8.22	18.5	849.8
F3		0.1	0.021	1.3e+003	8.22	18.5	849.8
G3		0.1	0.021	1.3e+003	8.22	18.5	849.8
H3		0.1	0.058	2.2e+003	8.2	26.6	732.6
I3		0.1	0.23	4.33e+003	8.2	47.3	649.70
A4	1	0.5	0.1040	6.49e+003	8.22	61.1	2.80e+003
B4		0.5	0.1040	6.49e+003	8.22	61.1	2.80e+003
C4		0.5	0.1040	6.49e+003	8.22	61.1	2.80e+003
D4		0.5	0.1040	6.49e+003	8.22	61.1	2.80e+003
E4		0.5	0.1040	6.49e+003	8.22	61.1	2.80e+003
F4		0.5	0.1040	6.49e+003	8.22	61.1	2.80e+003
G4		0.5	0.1040	6.49e+003	8.22	61.1	2.80e+003

H4		0.5	0.2890	1.08e+004	8.22	99.2	2.73e+003
I4		0.5	1.16	2.17e+004	8.22	191.7	2.63+003
A5	5	0.5	0.1040	6.49e+003	8.22	61.1	2.80e+003
B5		0.5	0.1040	6.49e+003	8.22	61.1	2.80e+003
C5		0.5	0.1040	6.49e+003	8.22	61.1	2.80e+003
D5		0.5	0.1040	6.49e+003	8.22	61.1	2.80e+003
E5		0.5	0.1040	6.49e+003	8.22	61.1	2.80e+003
F5		0.5	0.1040	6.49e+003	8.22	61.1	2.80e+003
G5		0.5	0.1040	6.49e+003	8.22	61.1	2.80e+003
H5		0.5	0.2890	1.08e+004	8.22	99.2	2.73e+003
I5		0.5	1.16	2.17e+004	8.22	191.7	2.63+003
A6	10	0.5	0.1040	6.49e+003	8.22	61.1	2.80e+003
B6		0.5	0.1040	6.49e+003	8.22	61.1	2.80e+003
C6		0.5	0.1040	6.49e+003	8.22	61.1	2.80e+003
D6		0.5	0.1040	6.49e+003	8.22	61.1	2.80e+003
E6		0.5	0.1040	6.49e+003	8.22	61.1	2.80e+003
F6		0.5	0.1040	6.49e+003	8.22	61.1	2.80e+003
G6		0.5	0.1040	6.49e+003	8.22	61.1	2.80e+003
H6		0.5	0.2890	1.08e+004	8.22	99.2	2.73e+003
I6		0.5	1.16	2.17e+004	8.22	191.7	2.63+003
A7	1	1	0.2081	1.2988e+004	8.22	110.1	5.0469e+003
B7		1	0.2081	1.2988e+004	8.22	110.1	5.0469e+003
C7		1	0.2081	1.2988e+004	8.22	110.1	5.0469e+003
D7		1	0.2081	1.2988e+004	8.22	110.1	5.0469e+003
E7		1	0.2081	1.2988e+004	8.22	110.1	5.0469e+003
F7		1	0.2081	1.2988e+004	8.22	110.1	5.0469e+003
G7		1	0.2081	1.2988e+004	8.22	110.1	5.0469e+003
H7		1	0.580	2.16e+004	8.22	178.9	4.9196e+003
I7		1	2.31	4.33e+004	8.22	345.6	4.7520e+003
A8	5	1	0.2081	1.2988e+004	8.22	110.1	5.0469e+003
B8		1	0.2081	1.2988e+004	8.22	110.1	5.0469e+003
C8		1	0.2081	1.2988e+004	8.22	110.1	5.0469e+003
D8		1	0.2081	1.2988e+004	8.22	110.1	5.0469e+003
E8		1	0.2081	1.2988e+004	8.22	110.1	5.0469e+003
F8		1	0.2081	1.2988e+004	8.22	110.1	5.0469e+003
G8		1	0.2081	1.2988e+004	8.22	110.1	5.0469e+003
H8		1	0.580	2.16e+004	8.22	178.9	4.9196e+003
I8		1	2.31	4.33e+004	8.22	345.6	4.7520e+003
A9	10	1	0.2081	1.2988e+004	8.22	110.1	5.0469e+003
B9		1	0.2081	1.2988e+004	8.22	110.1	5.0469e+003
C9		1	0.2081	1.2988e+004	8.22	110.1	5.0469e+003
D9		1	0.2081	1.2988e+004	8.22	110.1	5.0469e+003
E9		1	0.2081	1.2988e+004	8.22	110.1	5.0469e+003
F9		1	0.2081	1.2988e+004	8.22	110.1	5.0469e+003

G9		1	0.2081	1.2988e+004	8.22	110.1	5.0469e+003
H9		1	0.580	2.16e+004	8.22	178.9	4.9196e+003
I9		1	2.31	4.33e+004	8.22	345.6	4.7520e+003

For calculations concerning case A, D, G, the following geometric specifications were used

Table 14. Geometric specifications for cases A, D, and G

L	110 cm
Lc	100 cm
Do/Dr/Dc	40 cm
Da	10 cm
di	12 mm

<u>Vita</u>

Yuvraj Singh is the son of Nirmal and Sumanjeet Singh, born on September 4th, 1987. He completed his BS in Bioengineering at Lehigh University in 2010 and is currently pursuing his masters in Mechanical Engineering.